

1 **Greenland Blocking Index daily series 1851-2015: analysis of changes in extremes**  
2 **and links with North Atlantic and UK climate variability and change**

3 Short title: Greenland Blocking Index daily series 1851-2015

4 **MS accepted 27 February 2018 by *International Journal of Climatology***

5

6 Edward Hanna<sup>1</sup>, Richard J. Hall<sup>1</sup>, Thomas E. Cropper<sup>2</sup>, Thomas J. Ballinger<sup>3</sup>, Leanne  
7 Wake<sup>4</sup>, Thomas Mote<sup>5</sup>, John Cappelen<sup>6</sup>

8

9 <sup>1</sup>School of Geography and Lincoln Centre for Water & Planetary Health, University of  
10 Lincoln, UK

11 <sup>2</sup>School of Earth and Ocean Sciences, Cardiff University, Wales, UK

12 <sup>3</sup>Department of Geography, Texas State University, USA

13 <sup>4</sup>Department of Geography and Environmental Sciences, Northumbria University, UK

14 <sup>5</sup>Department of Geography, University of Georgia, USA

15 <sup>6</sup>Danish Meteorological Institute, Copenhagen, Denmark

16

17

18

19

20

21

22

23 **Corresponding Author:** Edward Hanna, School of Geography, University of Lincoln,

24 Think Tank, Roston Way, Lincoln, LN6 7FL, UK, [ehanna@lincoln.ac.uk](mailto:ehanna@lincoln.ac.uk)

25 **Abstract**

26

27 We present a homogenised Greenland Blocking Index (GBI) daily record from 1851-  
28 2015, therefore significantly extending our previously published monthly/seasonal GBI  
29 analysis. This new time series is analysed for evidence of changes in extreme events,  
30 and we investigate the underlying thermodynamic and dynamic precursors. We compare  
31 occurrences and changes in extreme events between our GBI record and a recently  
32 published, temporally similar daily North Atlantic Oscillation (NAO) series, and use  
33 this comparison to test dynamic meteorology hypotheses relating negative NAO to  
34 Greenland Blocking. We also compare daily GBI changes and extreme events with  
35 long-running indices of England and Wales temperature and precipitation, to assess  
36 potential downstream effects of Greenland blocking on UK extreme weather events and  
37 climate change. In this extended analysis we show that there have been sustained  
38 periods of positive GBI during 1870-1900 and from the late 1990s to present. A  
39 clustering of extreme high GBI events since 2000 is not consistently reflected by a  
40 similar grouping of extreme low NAO events. Case studies of North Atlantic  
41 atmospheric circulation changes linked with extreme high and low daily GBI episodes  
42 are used to shed light on potential linkages between Greenland blocking and jet-stream  
43 changes. Particularly noteworthy is a clustering of extreme high GBI events during mid-  
44 October in four out of five years during 2002-2006, which we investigate from both  
45 cryospheric and dynamic meteorology perspectives. Supporting evidence suggests that  
46 these autumn extreme GBI episodes may have been influenced by regional sea-ice  
47 anomalies off west Greenland but were probably largely forced by increases in Rossby-  
48 wave train activity originating from the tropical Pacific. However, more generally our

49 results indicate that high GBI winter anomalies are co-located with sea-ice anomalies,  
50 while there seems to be minimal influence of sea-ice anomalies on the recent significant  
51 increase in summer GBI.

52

53 **Keywords:** blocking, climate change, Greenland, jet stream, North Atlantic Oscillation,

54 UK

55

56

57

58

59

60

61

62

63

64

65

66

67

68

69

70

71

72

73

74 **1. Introduction**

75

76 Greenland high-pressure blocking is a key measure of changes in North Atlantic and  
77 Northern Hemisphere atmospheric circulation and potential Arctic-mid latitude climate  
78 linkages (e.g. Woollings et al. 2008, Davini et al. 2012a, Hall et al. 2015, Hanna et al.  
79 2015 & 2016, Mattingly et al. 2015, McLeod & Mote 2016, Overland et al. 2015 &  
80 2016, Budikova et al. 2017, Ballinger et al. 2018a). Blocking is generally used to  
81 describe a large, quasi-stationary mid-latitude anticyclone that persists for at least a few  
82 days, and is associated with increased large-scale meridional flow (Rex 1950), but there  
83 is no clear consensus on an exact definition (e.g. Woollings et al. 2008). Greenland  
84 blocking events tend to be characterised by cyclonic upper-level Rossby wavebreaking,  
85 which distorts the climatological trough south of Greenland and if it persists for a few  
86 days transfers relatively warm subtropical air masses to high northern latitudes over  
87 Greenland (Woollings et al. 2008, Davini et al. 2012a, Hanna et al. 2016). Cyclonic  
88 wavebreaking also favours episodes of extreme poleward moisture transport along the  
89 west coast of Greenland (e.g. Liu and Barnes 2015). These events have been observed  
90 to co-occur with Greenland Ice Sheet (GrIS) melt episodes, including the extreme July  
91 2012 melt event (e.g. Neff et al. 2014, Bonne et al. 2015). Since Greenland blocks  
92 typically lie well to the north of the jet stream they tend to divert rather than block the  
93 prevailing westerly airflow (DeWeaver & Nigam 2000, Luo et al. 2007a, Woollings et  
94 al. 2008, Davini et al. 2012a). The North Atlantic polar jet stream typically lies further  
95 south under blocked conditions (Hall et al. 2015), although bifurcated jet-stream

96 conditions, with one branch going further north than normal over Greenland as in  
97 summer 2007, are also possible (e.g. Hanna et al. 2009, their Figs. 14 & 15).

98 Greenland blocking events last on average for ~6-9 days, develop from the  
99 retrogression of an unusually strong Atlantic ridge, and are sometimes preceded by  
100 European blocking (Davini et al. 2012a). McLeod & Mote (2015) linked the intensity of  
101 extreme Greenland blocking episodes since 1979 to precursor cyclones, which formed  
102 to the west of Greenland prior to the occurrence of peak blocking. Greenland blocking  
103 is heavily influenced by the underlying Greenland landmass and topography (with the  
104 mountainous ice sheet rising up to ~3 km above sea-level). The high north-south-  
105 oriented Greenland topography causes atmospheric ridging, and surface cooling by the  
106 ice sheet and adjacent snow cover can produce high air pressure near the surface, with  
107 anticyclonic curvature often observed in cirrus cloud features, making Greenland one of  
108 the sunniest regions for its latitude (Scorer 1988). As relatively cold dense air spills out  
109 from the surface as katabatic drainage (e.g. Orr et al. 2005), air sinks from higher levels  
110 to fill the void, which can cause heating and raised geopotential heights aloft.

111 Strong Greenland blocking episodes have been linked to exceptional surface  
112 melting of the GrIS (Hanna et al. 2014, Tedesco et al. 2016a), record wet weather in  
113 large parts of the UK in summers 2007 and 2012 (Overland et al. 2012, Hanna et al.  
114 2016), and the highly unusual westward track of a major Hurricane (Sandy) which hit  
115 the US seaboard near New York in late October 2012 (Mattingly et al. 2015). Ballinger  
116 et al. (2018a) invoked increased Greenland blocking in autumn since 1979 to explain  
117 greater poleward transport of relatively warm air and reduced Baffin Bay sea-ice  
118 conditions, and coastal air temperature warming. Recent work also suggests an  
119 autumn/early winter Baffin Bay-Davis Strait-Labrador Sea (BDL) ice influence on the

120 thermal high and Greenland blocking, which is not supported in spring/summer melt  
121 periods (Ballinger et al. 2018b). This involves surface warming over the BDL region, a  
122 weakening of prevailing westerly winds, and a pronounced westward movement of the  
123 Greenland block (Chen & Luo 2017). Greenland blocking, which can also be influenced  
124 by surface meteorological and glaciological changes over the ice sheet (Hanna et al.  
125 2016), is therefore likely to have impacts on extreme weather and climate change over  
126 wide areas of the mid-latitude North Atlantic and areas well beyond Greenland.

127         Changes in Greenland blocking have recently been measured using the  
128 Greenland Blocking Index (GBI), which is defined using the mean 500 hPa (mid-  
129 tropospheric) geopotential height over the Greenland region of 60-80°N, 20-80°W  
130 (Fang 2004, Hanna et al. 2013, 2014, 2015 & 2016, Mattingly et al. 2015, McLeod &  
131 Mote 2015 & 2016) (Figure S1). Hanna et al. (2016) presented a long-running,  
132 homogenised monthly and seasonal GBI record based on a merging of the Twentieth  
133 Century Reanalysis Version 2c (hereafter 20CRv2c; Compo et al. 2011 & 2015) and  
134 NCEP/NCAR Reanalysis 1 (Kalnay et al. 1996), through post-processing that used  
135 splicing and breakpoint analysis. From their analysis, Hanna et al. (2016) found a  
136 significantly increasing GBI trend in summer in the last 1-3 decades that they ascribed  
137 to the Arctic amplification of global warming (Overland et al. 2016). Over this recent  
138 period, Hanna et al. (2016) also found that GBI had become significantly more variable  
139 from year to year in December: the cause of which remains uncertain but is related to a  
140 similarly more variable North Atlantic Oscillation (NAO) and Arctic Oscillation for the  
141 same calendar month (Hanna et al. 2015, Overland & Wang 2015). McLeod & Mote  
142 (2016) found an unusually high occurrence of extreme Greenland blocking episodes  
143 during 2007-2013, mainly in summer, compared with the rest of their 56-year record.

144           These previous studies are confined to analysing either daily or monthly and  
145 seasonal GBI changes since 1948. It is important to extend these observational analyses  
146 of recent Greenland blocking changes, given current uncertainty in the representation by  
147 climate models of North Atlantic jet-stream and blocking changes and potential Arctic  
148 climate-mid latitude weather linkages (Hall et al. 2015, Barnes & Screen 2015,  
149 Overland et al. 2016, Hanna et al. 2017).

150           Here we extend the work of Hanna et al. (2016) to present a fully homogenised  
151 daily GBI record from 1851-2015, relate extreme daily GBI events to atmospheric  
152 circulation and surface heating anomalies, and analyse our new record for evidence of  
153 any significant changes in the frequency of daily GBI episodes that may be related to  
154 climate change and have potential interactions with – and impacts on – mid-latitude  
155 North Atlantic circulation conditions south of and downstream of Greenland, including  
156 over the UK region. We examine the relationship between daily GBI and NAO over the  
157 seasonal cycle, compare relative changes in extreme daily GBI and NAO events within  
158 the last 165 years, and relate extreme daily GBI events to anomalous UK seasonal  
159 weather. We use our new, long homogenised daily GBI series together with a recently-  
160 published long NAO daily series to test the following dynamic meteorology hypotheses.  
161 These include the proposal by Woollings et al. (2008) that negative NAO is simply a  
162 high frequency of Greenland blocking events, and a positive NAO is the lack of such an  
163 event. Alternatively, Barriopedro et al. (2008) suggested that NAO changes may drive  
164 North Atlantic blocking trends. A further interpretation by Luo et al. (2007b) suggests  
165 that, since on the weekly timescale Greenland blocking and the negative phase of NAO  
166 events have the same spatial structure and lifetime characteristics, negative NAO events  
167 are identical to Greenland blocking episodes rather than arising from or driving the

168 latter. Finally we also consider how the recent marked autumn/winter sea-ice decline  
169 west of Greenland, and the state of the North Pacific atmospheric jet further upstream,  
170 may affect Greenland blocking and the North Atlantic jet.

171 Section 2 describes the datasets and statistical analysis methods used in this  
172 study, Section 3 summarises the results, which are presented by monthly/seasonal and  
173 then extreme daily GBI analyses in turn; a discussion and summary of the results is  
174 provided in Section 4.

175

## 176 **2. Datasets and methods**

177

178 Greenland Blocking Index (GBI) daily data for 1948-2015 were calculated based on  
179 NCEP/NCAR reanalysis 500 hPa geopotential height data downloaded for a grid of 35  
180 well distributed points (Figure S1), which were then averaged to produce daily values  
181 for the standard GBI region of 60-80°N, 20-80°W. Older daily GBI data for 1851-1947  
182 were derived from the 20CRv2c (Compo et al. 2015), but needed homogeneity  
183 adjustments and splicing against the NCEP/NCAR-based GBI record for the common  
184 overlap period. The same homogenisation and splicing methods and coefficients used  
185 for the monthly series (Hanna et al. 2016) are applied to the daily series.

186 We adjusted the NCEP/NCAR daily GBI values because the National  
187 Oceanographic & Atmospheric Administration Earth Systems Research Laboratory  
188 Physical Sciences Division (NOAA ESRL PSD) online web tool at  
189 <https://www.esrl.noaa.gov/psd/data/timeseries/daily/> only allows daily data to be  
190 downloaded for points rather than areas. We acquired data for every 5° latitude and 10°  
191 longitude over the GBI region (35 points in total) but this gives an area-weighting



192 towards high northern latitudes (denser coverage of points) that needs correcting. This  
193 was done using regression splicing of monthly means of the 35-point daily time series  
194 against the full area-averaged, area-weighted monthly time series downloaded  
195 separately, with excellent agreement between the adjusted daily NCEP/NCAR GBI  
196 series and the original monthly NCEP/NCAR GBI series.

197 Each GBI daily value was then normalised with respect to the mean and  
198 standard deviation of all the daily GBI values for 1951-2000 for that day of year. This  
199 procedure provides the advantage of avoiding occasional jumps between months that  
200 would otherwise have arisen from the use of monthly coefficients derived in our  
201 previous analysis. Monthly means of daily 20CRv2c and NCEP/NCAR GBI agree  
202 extremely well ( $r=0.92-0.99$ ) for the 1948-2014 overlap period. Daily data are an  
203 extension of monthly GBI time series presented in Hanna et al. (2016).

204 McLeod & Mote (2016) define an extreme GBI event as having at least 5  
205 consecutive days where the GBI attained at least the 97<sup>th</sup> percentile of all 1958-2013  
206 daily GBI values for a 7-day window centred on that date. However, unlike McLeod &  
207 Mote (2016), we do not pre-process the data using a low-pass filter, as we prefer to  
208 preserve the high-frequency GBI signal. We instead take extreme daily GBI events as  
209 being above or below certain thresholds (e.g. 2 or 3 standard deviations ( $\sigma$ ) above or  
210 below the respective long-term mean for that day of year), and analyse changes in the  
211 frequency of these events with time. We focus initially on GBI events exceeding  $3\sigma$  for  
212 at least three consecutive days, as they are statistical outliers and represent a  
213 manageable number of extreme events.

214 We also co-analyse extreme GBI episodes in comparison with changes in  
215 extreme daily NAO events, based on a temporally comparable Azores-Iceland station-

216 based NAO dataset (Cropper et al. 2015, hereafter abbreviated C15), supplemented with  
217 the Climate Prediction Centre (CPC)'s principal component-based daily NAO index for  
218 the period since 1950 (Barnston & Livezey 1987;  
219 <http://www.cpc.ncep.noaa.gov/products/precip/CWlink/pna/nao.shtml> ), and with North  
220 Atlantic polar jet stream daily speed and position (Hall et al. 2015; Hall, 2016). Jet  
221 speed and position are calculated using the method of Woollings et al. (2010) applied to  
222 20CRv2c data. Mean daily zonal wind speeds over the North Atlantic (0-60W,16-76N)  
223 are averaged over 900-700 hPa. A zonal mean wind speed is then calculated for each 2°  
224 latitude band, and these zonal means are low-pass filtered using a 61-point Lanczos  
225 filter to remove synoptic scale (<10 days) variability (Duchon, 1979). The latitude band  
226 with the maximum mean zonal wind speed for each day is taken as the jet latitude, and  
227 the zonal mean wind speed at that latitude is the jet speed. Monthly and seasonal  
228 averages are calculated for each jet metric.

229 To test the hypothesis of Woollings et al. (2008) outlined above, we first  
230 compare the numbers of days per month above or below various GBI values with  
231 monthly mean NAO values and with the numbers of days per month that have NAO  
232 values of similar magnitude but opposite sign (i.e. the numbers of GBI>2 days are  
233 compared with numbers of NAO<-2 days for each month and season). We also compare  
234 the numbers of moderate (<-1 & >1 $\sigma$ ) and extreme (<-2 & >2 $\sigma$ ) NAO days with  
235 monthly mean GBI values. Second, we determine any leads and lags between respective  
236 changes in GBI, NAO and North Atlantic jet stream metrics in the extreme GBI event  
237 daily case studies mentioned above. To help elucidate NAO-GBI interactions we  
238 investigate seasonal composites of 500 hPa geopotential height anomalies over  
239 Greenland for daily NAOI negative values below stepped NAOI thresholds [i.e. a

240 composite (mean) of days with NAO values where  $-1.5\sigma < -1\sigma$ , then further composites  
241 with progressively more extreme z-values in  $-0.5\sigma$  steps], based on 20CRv2c data  
242 spanning 1850-2014.

243 We additionally use 20CRv2c composite plots of 500 hPa geopotential height  
244 and vector winds, alongside 850 hPa temperature anomalies for seasons and months  
245 having the highest numbers of moderately high GBI (GBI>1) days. Since these plots are  
246 based on 1851-2014, they represent nearly the full period of GBI record. Hadley Centre  
247 Sea Ice and Sea Surface Temperature (HadISST) sea-surface temperature (Rayner et al.  
248 2003) and HadISST2.2 sea-ice data (Titchner & Rayner 2014) are used to elucidate  
249 GBI-sea ice relationships on the regional basis around Greenland.

250 Finally we compare our GBI daily series with daily time series of both Central  
251 England Temperature (CET; Parker et al. 1992) and England & Wales Precipitation  
252 (EWP; Alexander & Jones 2001), where these long-running and well-documented  
253 meteorological records allow us to track the potential impact of GBI changes for most  
254 of the period of record on North Atlantic polar jet-stream conditions over the UK, i.e.  
255 downstream of Greenland.

256 Pearson's product-moment correlation, bivariate linear regression and composite  
257 analyses are the main statistical methods used here. Statistical significance of calculated  
258 trends is tested using an online t-test calculator  
259 <http://www.graphpad.com/quickcalcs/pvalue1.cfm> based on Abramowitz & Stegun  
260 (1965). Statistical significance is defined using a standard  $p \leq 0.05$  threshold. Datasets  
261 are de-trended prior to carrying out correlation.

262 The analysis covers all months but – because of a mass of data – focuses on key  
263 summer and winter months (June, July and December) for which intriguing changes in

264 North Atlantic atmospheric circulation have recently been identified, especially for the  
265 period of rapid Arctic sea-ice decline since 2007 (Serreze & Stroeve 2015); these  
266 changes include a more meridional jet-stream flow in early summer and increased  
267 variability in circulation metrics during December (Overland et al. 2012; Hanna et al.  
268 2015 & 2016; Overland & Wang 2015). Standard 3-month meteorological seasons are  
269 used (DJF, MAM, JJA, SON). Throughout the paper, where seasonal data/analysis are  
270 discussed, winter (DJF) seasons are denoted by the year of the January.

271

### 272 **3. Results**

273

#### 274 3.1 Monthly and seasonal GBI analysis

275

##### 276 *3.1.1 Long-term/secular changes in GBI and NAO*

277

278 Cumulative annual and monthly totals of daily GBI are shown in Figure 1. The annual  
279 data show upward inflections in the cumulative GBI curve from ~1870-1900 and  
280 ~2000-2015, and a decline during 1970-1990. These features are also apparent in the  
281 cumulative time series for the summer months but are largely absent in winter. The  
282 recent (post-2000) accumulation of high GBI daily values is particularly strong for  
283 August relative to June and July. September also shows a similarly striking recent  
284 increase to the summer months, while October and November do not. This therefore  
285 reflects an inter-seasonal summer progression of this interannual change. There is less  
286 secular change in other seasons compared with summer, although January and April  
287 show marked long-term declines in GBI.

288 Mean numbers of GBI days for different thresholds (GBI>0,1,2; NAO<0,-1,-2)  
289 for each calendar month, year and summer and winter seasons are summarised in Tables  
290 1, S1 & S2. These show clusterings of high numbers of GBI days for summer and the  
291 year as a whole for the last decade (2006-2015) relative to the climatological mean. For  
292 example the number of summer days with GBI values >0 (>1) is 69.5 (35.6) relative to  
293 (1981-2010) climatological means of 47.7 (18.6) [Table S1(a) & Table 1]. The  
294 difference is even more striking for number of summer days having GBI>2 (10.0  
295 relative to 3.8) (Table S1b). However, other months do not have record numbers of  
296 positive /high-value GBI days at the end of the period: for example, January, December  
297 and winter (May and September) generally have record numbers of such days during the  
298 1960s (1950s and 1930s respectively), while October and November generally have  
299 their greatest numbers of positive GBI days during the second half of the Nineteenth  
300 Century (Tables 1 & S1a). In contrast, Table S2 showing changes in numbers of station-  
301 based NAO days, does not show any recent (post-2000) record clusterings of  
302 negative/low-value NAO days, except (marginally) for December 2000-2009 for  
303 NAO<-1,-2. This may be related to the use of a station-based NAO index in summer  
304 since the PC-based NAO index does show recent clusterings of low NAO index days in  
305 summer (Table S3). However, there is a pattern where certain months with high  
306 numbers of positive GBI days for particular decades show correspondingly high  
307 numbers of negative NAO days for the same months/decades (e.g. January and winter  
308 for the 1960s; March, 1950s).

309 A visualisation of changes in numbers of annual and summer and winter  
310 seasonal GBI and NAO days is shown in Figures 2 and S2. These graphs show little  
311 change in numbers of GBI>0 days, but clear upward trends in numbers of more extreme

312 GBI>1,2 days, for the period as a whole (Figure 2a-c). However, overall trends are  
313 significant only in 3/6 cases: for summer for moderately high GBI>1 episodes, and for  
314 winter and annual for more extreme GBI>2 events. The 2010 record peak in annual  
315 GBI>2 days is only slightly above previous similar peaks in 1878 and 1887, while 2008  
316 and 2011 peaks in summer GBI>2 days are preceded by several similar peaks during the  
317 early Twentieth Century. Regarding the number of GBI>1 days, there are recent  
318 exceptional peaks in all three series: 2010 (annual and winter) and 2012 (summer). By  
319 contrast, Figure S2 shows few cases and insignificant trends in negative NAO days, and  
320 that peaks in such events in the last decade are unexceptional in the context of the  
321 overall NAO record.

322         These results are supported by the trend analysis for summer and winter and  
323 selected months presented in Table 2, which clearly shows many significantly positive  
324 GBI trends for the recent 1990-2015 period but relatively few trends for longer/earlier  
325 and intermediate periods (Table 2a). Within the last 26 years, significant upward trends  
326 in numbers of GBI days>0,1 are almost ubiquitous for summer and annual series but are  
327 less consistent for winter data. Also of note is a significant increase in the annual  
328 number of days with GBI>1 since 1900. There were few sustained changes in the  
329 monthly or seasonal standard deviation of daily GBI values during the period of record.  
330 A similar analysis of trends in numbers of days with negative NAO values (Table S4)  
331 indicates no significant trends after 1990, corroborating the earlier results from Tables  
332 1, S1 and S2: i.e. recent increasingly common high GBI days (which are primarily a  
333 summer phenomenon) have not been generally mirrored by more frequent low NAO  
334 days. Again, this apparent breakdown in the relation between high GBI and low NAO is

335 likely to be linked to our primary use of a station-based NAO series rather than  
336 necessarily indicating a real breakdown in the GBI-NAO relation.

337         Next we examine rank-ordered numbers of high GBI ( $GBI > 1$ ) days for selected  
338 summer and winter seasons (Table 3). Two recent years 2012 and 2010 stand out as  
339 having exceptionally high numbers of positive GBI days in summer and winter  
340 respectively, in accordance with previous work finding record high values in these years  
341 based on seasonal GBI data (Hanna et al. 2016). However, it is also clear from this table  
342 that, despite there being some relation, there is not always a clear correspondence  
343 between the numbers of high GBI and low NAO days for particular months and years.  
344 For example, June had the greatest number of  $GBI > 2$  days in 1891 and 1897 but the  
345 greatest number of  $NAO < -2$  days was in 1903. Also, 1911, which had some of the  
346 greatest numbers of  $NAO < -1, -2$  days in summer, had a smaller number of positive GBI  
347 values than several other summers.

348

### 349 *3.1.2 GBI relation with NAO*

350

351 Figure 3 summarises correlations between daily GBI and NAO values for the full  
352 (1851-2015) period, including variations in mean daily correlations over the seasonal  
353 cycle (i.e. correlation calculated for 1 January for all years, then repeated for each day  
354 of year; Figure 1a,b) and interannually (correlation calculated for 1851 for all days, then  
355 repeated for all years; Figure 1c). These generally indicate the strongest correlations  
356 during winter and spring, and weakest correlations (although all still significant) in  
357 summer. GBI-NAO correlations are typically  $\sim -0.6$  but range from  $\sim -0.4$  in mid-  
358 summer to  $\sim -0.7$  in late winter and early spring. Figure 3(b) is similar to Figure 3(a) but

359 includes both station-based and principal-component based (CPC) NAO indices for the  
360 1950-2015 common period. Inter-seasonal correlations hold up well, and actually  
361 increase slightly in summer, when the CPC NAO series is used. This indicates that the  
362 summer drop-off in seasonal correlations is due to use of a station-based NAO index  
363 that does not fully capture migration of the NAO centres of action (i.e. the regions of  
364 maximum surface pressure change) rather than a real physical weakening of the GBI-  
365 NAO relation. Regarding long-term changes, Figure 3(c) shows that correlations are  
366 notably lower for the pre-1880 period, which may reflect limitations with these early  
367 parts of the GBI and NAO series, and especially in the realistic representation of mid-  
368 tropospheric geopotential height variations over Greenland at the daily timescale. For  
369 example, 20CRv2c globally-averaged geopotential fields before about 1865 appear to  
370 be biased low by errors in marine pressure observations that were assimilated by the  
371 reanalysis  
372 ([https://www.esrl.noaa.gov/psd/data/gridded/20thC\\_ReanV2c/opportunities.html](https://www.esrl.noaa.gov/psd/data/gridded/20thC_ReanV2c/opportunities.html)).

373 Alternatively, gridded sea-level-pressure fields were used instead of meteorological  
374 station data as a basis for constructing the C15 daily NAO series from the 1850s to the  
375 early 1870s, with the latter time marking a jump in the running correlations.

376 Monthly and seasonal correlation coefficients between numbers of days per  
377 month or season above or below specified GBI thresholds and (a) monthly or seasonal  
378 mean GBI, (b) monthly or seasonal mean NAO and (c) numbers of days per month or  
379 season above and below NAO thresholds of opposite sign and magnitude are shown in  
380 Table 4. Subset (a) shows very strong ( $r \geq 0.90$ ) correlations between mean GBI and  
381 numbers of positive GBI days ( $GBI > 0$ ) for all months and seasons listed. The  
382 correspondence is almost as strong for numbers of  $GBI > 1$  days (0.88 for annual) and



383 still 0.72 (-0.77) for numbers of GBI >2 (<-1) days but is much less strong at -0.48  
384 (annual) for GBI<-2 days. There is also generally good agreement between numbers of  
385 thresholded GBI days and monthly or seasonal mean NAO, which is strongest for  
386 GBI>1 values (e.g. -0.81 for winter and -0.44 for summer), and almost as strong for  
387 GBI>2 values. The correspondence is a lot less strong for thresholded negative GBI  
388 values, falling to  $r = 0.21$  (0.06) for winter (summer) based on the GBI<-2 value subset.  
389 Correlations of numbers of GBI days above or below given thresholds with monthly  
390 mean NAO are consistently weaker for summer relative to winter (Table 4b). Table 4(c)  
391 indicates generally good correspondence between numbers of high (low) GBI and low  
392 (high) NAO events (e.g.  $r = 0.64$  for annual data). However, following the above  
393 pattern, there is less agreement between numbers of extreme negative GBI (GBI<-2)  
394 days and numbers of extreme positive NAO (NAO>2) days ( $r = 0.23$ ). Table 4(d)  
395 confirms the above pattern by showing a stronger (less strong) association between  
396 numbers of extreme negative (positive) NAO days and monthly or seasonal mean GBI  
397 values.

398 Our stepped threshold analysis of geopotential height anomalies and patterns for  
399 successively more negative NAO1 conditions shows high GPH500 clearly linked with  
400 Greenland blocking, i.e. the anomalies are centred over Greenland, in winter (Figure  
401 S3). In summer the highest GPH500 anomalies are offset to be centred between  
402 Greenland and Iceland, and are centred near Iceland for the lowest NAO cases (<-3.5 $\sigma$ ).  
403 The weaker summer GPH500 anomalies and the eastward shift in the NAO pattern are  
404 likely to be responsible for the NAO-GBI relation in summer being generally less strong  
405 than in winter (Table 4). Winter low NAO (high GBI) cases are associated with low

406 GPH500 anomalies across much of central Europe, parts of Scandinavia and Russia but  
407 this is not the case for summer (Figure S3).

408

409

410 *3.1.3 GBI relation with Northern Hemisphere mid-high latitude circulation and sea-ice*  
411 *anomalies*

412

413 Composite plots showing anomalies of 500 hPa geopotential height (GPH500), vector  
414 winds, 850 hPa temperatures (T850), and sea-ice-concentration (SIC) for the five  
415 seasons/years with the highest numbers of GBI>1 days (years listed in Table 3), are  
416 shown in Figure 4. For summer (JJA) (Figure 4b), these show a GPH500 anomaly  
417 aligned SSW-NNE with a main focus ~70 m centred just off the southwest Greenland  
418 coast. Meanwhile, modest negative GPH500 anomalies of ~-20 m are located over  
419 Ireland and in the Atlantic just west of the UK. Low heights are also evident over  
420 western and northern Alaska and the Bering Strait. The corresponding composite vector  
421 wind anomaly plot shows a southward-displaced North Atlantic jet, with its core  
422 extending eastwards south of the UK, with stronger-than-normal westerlies over Biscay  
423 and north-east anomalies over much of the mid northern North Atlantic around Iceland  
424 and south of Greenland (Figure 4d). Warm air anomalies are located over west  
425 Greenland, the Labrador Sea and Canadian Archipelago, with a striking 3°C warm spot  
426 over extreme north Siberia near the coast (Figure 4f). This may reflect increased  
427 seasonal sea-ice depletion in these high GBI years, as the wind-vector anomaly plot  
428 shows an offshore (southerly) wind bias (Figure 4d). This is supported by SIC  
429 anomalies which are biased low in the same region during conditions of high GBI in

430 summer (Figure 4h). However, pockets of moderate SIC anomalies in coastal areas of  
431 Greenland and Baffin Bay suggest a minimal contribution of localised open-water  
432 anomalies to +GBI anomalies, although sea-surface temperatures (SSTs) are biased  
433 warm south of Greenland (Figure 4j). Advection of relatively cold Arctic air over the  
434 Bering Strait region may be responsible for the low GPH500 and T850 anomalies  
435 centred over Alaska, and this is also linked to cold SSTs in that region (Figures 4b,d,f,j).

436         Seasonal anomalies for the five winters with the greatest number of GBI>1 days  
437 (Table 3b) are now examined (Figure 4a,c,e,g,i). In comparison with summer, the top  
438 five winters show a much greater (about double the magnitude) and more zonally-  
439 aligned GPH500 anomaly, which extends further west over the Labrador Sea and  
440 Canadian Archipelago (Figure 4a). The high GPH500 anomaly extends towards  
441 Svalbard and over central Russia, rather than across the central Arctic Ocean as in  
442 summer, and there is a much wider swath of negative GPH500 heights and low pressure  
443 extending west-east entirely across the mid-Atlantic and into northern Europe, which is  
444 most intense over northern France and south-western parts of the UK. Anomalous  
445 southerly airflow extends north over the Canadian Arctic Archipelago, Labrador Sea  
446 and over west Greenland (Figure 4c). The corresponding T850 plot shows an intense  
447 warm spot centred over the Labrador Sea and Baffin Bay areas, and cold anomalies  
448 focused over Siberia, Scandinavia and much of eastern, central and northern-western  
449 US (Figure 4e). In contrast with the summer situation around Greenland, the SIC  
450 anomaly pattern in winter over parts of southern Baffin Bay, Davis Strait and the  
451 northern Labrador Sea (Figure 4g) appears co-located with the GPH500 anomaly shown  
452 in Figure 4a. The upper-level anticyclone is centred over a marginal ice zone  
453 characterised by anomalously low ice coverage, allowing upward heat fluxes from the

454 open ocean or young sea ice to sustain the ridge aloft. The enhanced near-surface  
455 warming weakens prevailing westerly winds via the thermal-wind principle and  
456 prolongs pre-existing Greenland blockings (Chen & Luo 2017). SST anomalies are  
457 generally high around south and west Greenland but are low immediately off the east  
458 and south-east coasts (Figure 4i).

459 3.2 Extreme GBI events on daily timescale – North Atlantic synoptic characteristics and  
460 precursors

461

462 GBI episodes of  $\geq 3(\leq -2.5)\sigma$  where these thresholds were attained or surpassed for at  
463 least three consecutive calendar days are summarised in Table 5. These events are  
464 concentrated in certain parts of the record: for example, with 1875-1900 and 2002-2010  
465 accounting for respectively 10 and 12 out of 32 anomalously high GBI events in Table  
466 5(a); these peak periods are in accordance with our cumulative daily GBI results  
467 reported in Section 3.1.1. Of particular note is a clustering of unusually high GBI  
468 episodes during mid-October in several successive years: 2002, 2003, 2005 and 2006  
469 (2004 October with three consecutive days having GBI values  $\geq 2.85$ , with the last two  
470 of these days  $\text{GBI} > 3$ , fell only slightly under the threshold). Is this unprecedented  
471 sequence of extreme GBI events just a statistical quirk or does it reflect a seasonally-  
472 sensitive physical forcing mechanism that has perhaps been triggered or exacerbated by  
473 Greenland climate change and sea-ice loss in the wider Arctic region?

474 To help set these extreme GBI episodes (Table 5) in a broader context and  
475 discern possible precursors and impacts, we analyse atmospheric circulation conditions  
476 and anomalies over the wider North Atlantic region and their evolution at the daily  
477 timescale for a period from 5 days before to 5 days after these episodes (Figure 5).

478 Mean synoptic conditions during the 2002, 2003, 2005 and 2006 October episodes  
479 indicate that the North Atlantic jet stream moved south by  $\sim 7^\circ$  latitude and first  
480 decreased its speed by  $\sim 25\%$  during the five days prior to the highest part of these  
481 October GBI phases but subsequently accelerated to above initial values during the time  
482 of peak GBI; although the C15 station-based Azores-Iceland NAO index showed an  
483 inverse but similar symmetric response to GBI, the principal-component-based CPC  
484 NAO index minimum is time-lagged by 2 or 3 days with respect to the peak in the GBI  
485 cycle (Figure 5a). There is a similar clustering of high GBI events in late September and  
486 October during the late Nineteenth and early Twentieth Centuries [1880 (x2), 1888,  
487 1895 and 1916; Table 5a], and a further graph shows the synoptic evolution of these  
488 earlier events (Figure 5b). The southward movement of the jet 3-5 days before the rise  
489 in Greenland blocking is evident but in this case there is little systematic change in jet  
490 speed, while – similar to the above - there does not seem to be any lag between the GBI  
491 maximum and the Azores-Iceland NAO minimum (there are no available CPC NAO  
492 data before 1950 for comparison purposes). A composite graph of high GBI episodes  
493 during summer (Figure 5c) shows the jet jumping south, with the main shift 2-3 days  
494 before peak GBI, but not much change in jet speed (a slight slowdown, then speed-up,  
495 of  $<10\%$ ). CPC NAO changes almost mirror the GBI changes, while the Azores-Iceland  
496 NAO reaches its minimum 4 days following peak GBI. The winter extreme high GBI  
497 composite (Figure 5d) shows the jet jumping south  $>10^\circ$  1 day before peak GBI but  
498 with little change in speed, while both NAO records approximately (inversely) mirror  
499 the GBI changes.

500           Turning our attention now to a notable clustering of extreme \*low\*/negative  
501 GBI events which occurred in the springs of 1897, 1906, 1934, 1990, 1993, 2011 and

502 2013 (Table 5b), the North Atlantic jet shifts north on average by  $\sim 9^\circ$  while  
503 simultaneously strengthening from  $\sim 12$  to  $16 \text{ m s}^{-1}$  from 3 days ahead of GBI minimum.  
504 The Azores-Iceland (CPC) NAO positively peaks  $\sim 1$  (2-5) days after the lowest  
505 negative GBI value (Figure 5e). Again, the jet typically shifts before the GBI reaches its  
506 most negative value, with the accompanying change in the NAO index tending to lag  
507 slightly behind.

508

### 509 3.3 Comparison of GBI and NAO daily series with UK climate indices

510

511 Daily GBI and C15 Azores-Iceland NAO series are correlated with CET and EWP UK  
512 climate indices for both the seasonal cycle and interannually for the full periods of  
513 overlapping records (1851-2015 for CET and 1931-2015 for EWP), in the same way as  
514 described for Figure 3 in Section 3.1.2, and the results are presented in Figure 6.  
515 Relatively weak correlations for CET range from  $\sim \pm 0.4$  in winter to near zero in  
516 summer, with correlations generally being of opposite sign for GBI and NAO (Figure  
517 6a). For the seasonal plots correlations greater than  $\pm 0.15$  are significant, so there is a  
518 fairly persistent positive (negative) association between CET and NAO (GBI) between  
519 November and April but correlations are insignificant for the rest of the year; also,  
520 annual mean correlations have been relatively stable for the last century and a half  
521 (Figure 6b). Winter 2009/10, which had a record high number of positive GBI days in  
522 the whole 165 years of record (Table 3b), was characterised by unusually cold, snowy  
523 winter weather over the UK (e.g. Hanna et al. 2017); the following winter 2010/11 also  
524 featured severe cold over the UK, including the coldest December CET since 1890, and  
525 has the fourth greatest number of highly positive winter GBI days. For EWP,

526 correlations with NAO and GBI are overall weaker but are again of opposite sign and  
527 are briefly and significantly positive for NAO in December and approach the  
528 significance threshold (positive) for GBI in summer; as for CET, there is no sign of a  
529 systematic shift of these correlations over time (Figure 6b,d). However, in summer  
530 CET/EWP correlations will be low with station-based NAO as the latter does not  
531 capture shifts in centres of action of the summer NAO regime (i.e. there is a significant  
532 seasonal shift in the locations of maximum surface pressure variation). Extreme positive  
533 GBI events tend to be associated with both relatively low CET and with moderate to  
534 high ( $>2 \text{ mm day}^{-1}$ ) EWP; conversely, extreme negative GBI episodes typically  
535 coincide with near- or above-average CET and generally lower EWP, with several  
536 notably high CET events in spring and summer values (Table 5). Notably, referring to  
537 the clearly record high numbers of positive GBI days in summer 2012 (Table 3a), this  
538 was a record-breaking wet summer in England and Wales – the wettest for a century –  
539 and was also cooler than average (Parry et al. 2013; Hanna et al. 2017).

540

#### 541 **4. Discussion/summary**

542

543 We have compiled, presented and analysed a new homogenised daily GBI dataset from  
544 1851-2015. This valuable extension enabled an analysis of high-time-frequency (daily)  
545 weather events, and their changing frequency/intensity in the context of changing  
546 climate. Long-term monthly and seasonal statistics have also been computed,  
547 reinforcing findings from a previous study (Hanna et al. 2016). Recent increases in the  
548 frequency of extreme high GBI events are noted for June, July and August (Table 1) but  
549 are not always mirrored by increases in low NAO episodes (Table S2b), although

550 results are sensitive to the type of NAO index used (Table S3b). Steep increases in  
551 cumulative daily GBI for 1870-1900 and 2000-2015 are noted for the overall annual  
552 time series and summer monthly series but are much more muted for winter monthly  
553 series (Figure 1). These GBI trends are broadly in line with our previous results based  
554 on monthly/seasonal GBI analysis (Hanna et al. 2016). The summer increase in  
555 cumulative daily GBI is much more marked for high summer (Figure 1), and this may  
556 result from cumulative positive feedbacks acting more strongly in August, relative to  
557 June and July, during progressively warmer Greenland summers since 2000 (Hanna et  
558 al. 2008, 2012, 2014; Tedesco et al. 2016b).

559       The comparisons between monthly counts of the number of thresholded GBI  
560 days and both the monthly mean NAO and numbers of thresholded NAO days are  
561 generally stronger for positive GBI and negative NAO (Table 4). Also there is a slight  
562 lag (mean ~1 day) between peak GBI and record NAO over a number of extreme daily  
563 events, although both the extreme GBI and NAO values tend to be preceded by a  
564 southward (northward) movement of the jet under positive (negative) GBI (Figure 5 &  
565 Table 5). Our findings generally support the Woollings et al. (2008) hypothesis that  
566 negative NAO arises from Greenland blocking and that positive NAO mainly represents  
567 the absence of blocking (rather than ‘anti-blocking’ or negative GBI conditions). This is  
568 also in agreement with the results of Davini et al. (2012b), who found that the first  
569 Empirical Orthogonal Function of the 500 hPa geopotential height over Europe and the  
570 North Atlantic did not resemble the NAO for GBI- cases but more closely resembled an  
571 East-Atlantic circulation pattern (e.g. Hall et al. 2015; Hall & Hanna 2018) and that  
572 North Atlantic jet variability was then no longer related to Greenland blocking changes.  
573 Also in support of our findings that high-GBI and low-NAO events do not always align,



574 Rimbu et al. (2017) found that stable-isotope variations in GrIS cores are more closely  
575 related to measures of Atlantic-European/Greenland blocking than the NAO index.

576 Our composite analysis of seasonally high GBI events (Figure 4) indicates a  
577 strong winter GBI signal linked to positive sea-surface temperature anomalies and  
578 negative sea-ice anomalies/freeze delays persisting into autumn. This relationship does  
579 not necessarily hold in spring when SSTs are relatively lower around the marginal ice  
580 zone west of Greenland as proximate air-sea fluxes tend to be negative (toward the  
581 surface) (Fenty & Heimbach 2013) including around the time of unseasonably early  
582 melt onset (Ballinger et al. 2018b). The winter co-location of high 500 GPH anomaly  
583 with low sea-ice anomalies suggests possible forcing in the form of ocean-atmosphere  
584 heat release through leads or new, thin ice cover, following the mechanism proposed in  
585 Ballinger et al. (2018a). Conversely, we have shown a likely minimal contribution of  
586 sea-ice anomalies to positive GBI anomalies in summer, while the relatively low  
587 summer air-sea temperature difference suggests a much more muted effect of SST  
588 anomalies around southern Greenland. On the basis of these results, we suggest that  
589 different mechanisms - relatively greater ocean-atmosphere heating in autumn - may  
590 enhance, or help sustain, blocking at these different times of year although this warrants  
591 further investigation.

592 Regarding the mid-2000s (2003-2006) clustering of extreme high GBI events in  
593 mid-October, we hypothesize that this may be related to the recent rapid loss of sea-ice  
594 to the west of Greenland, as the latest Baffin freeze dates since 1979 (i.e. 1 sigma  
595 events) have all occurred since 2002 (ranked 3<sup>rd</sup> latest) with 2006 marking the latest,  
596 and 2003 and 2005 freeze onset was later than normal ( $\geq +0.5$  sigma) (Markus et al.  
597 2009; Ballinger et al. 2018a). Three out of four of these years had reduced sea ice in the

598 northern part of Baffin Bay compared with 1979-2016 (ERA-I) climatology, although  
599 the pattern in 2005 was somewhat different, with a positive ice anomaly in much of the  
600 region (Figure S4). However, as these SIC anomalies are in confined areas typically  
601 characterised by low/thin ice coverage (climatological SIC=0.1-0.4), it is uncertain to  
602 what extent they may be responsible for such anomalous GBI values. Also, other years  
603 around that period, for example 2007 (Figure S4), have similar SIC anomalies but are  
604 not associated with anomalously high GBI. Nevertheless, we posit an autumn open-  
605 water linkage (south Baffin Bay, Davis Strait, north Labrador Sea) to extreme positive  
606 GBI, with possible upward heat contribution for north Baffin Bay in thinner-than-  
607 average years such as 2005.

608         Benedict et al. (2004) suggest that cyclonic (anticyclonic) wavebreaking  
609 displays a NW-SE (NE-SW) tilt. Under high GBI conditions, therefore, this tilt tends to  
610 deflect cyclones south (Priestly et al. 2017), which naturally gives rise to more negative  
611 NAO conditions, which over much of the UK are typically relatively cold and dry in  
612 winter but wet in summer (Hall & Hanna 2018). Rossby wave breaking in the east  
613 Atlantic is noted to precede the main/peak change in the jet stream in that region by ~2  
614 days, and this is in accordance with our finding that the NAO low point sometimes lags  
615 peak GBI by 1-2 days. Benedict et al. (2004) also suggest that the remnants of the  
616 wavebreaking, which originates from transient eddies from far upstream, form and  
617 maintain the NAO; when wavebreaking stops, the NAO phase decays. Therefore the  
618 GBI may be remotely forced, or at least influenced, from as far afield as the Pacific,  
619 rather than simply locally formed. This might be especially important for the negative  
620 NAO (positive GBI) phase, as suggested by Ding et al. (2014) and Trenberth et al.  
621 (2014). According to their hypothesis, a Rossby-wave train could act to transmit SST

622 signals from the central Pacific to Greenland and north-east Canada, and the high GBI  
623 events are primarily an adiabatic response to concomitant changes in the upper-  
624 troposphere circulation. Moreover there is mounting evidence that - in advecting energy  
625 and moisture polewards - such planetary wave trains may influence Arctic sea-ice cover  
626 (Yoo et al. 2012, Park et al. 2015, Baggett & Lee 2017, Ding et al. 2017) and therefore  
627 Greenland blocking.

628         This concept of tropical Pacific forcing of Greenland blocking is supported by  
629 evidence of equatorward perturbations of the North Pacific jet prior to the extreme high  
630 October (2002-2006) GBI episodes (Figure S5), consistent with Franzke et al. (2004). In  
631 addition, three of the four extreme October positive GBI events (2002, 2005 & 2006)  
632 were preceded by anomalous high pressure over Scandinavia, which is consistent with  
633 anomalous European blocking sometimes being a precursor of Greenland blocking  
634 (Davini et al., 2012a, McLeod and Mote, 2015). While a sample of four events is far  
635 from conclusive, these upstream and downstream dynamical associations suggest that  
636 the coincident extreme GBI events in October are unlikely to be more solely forced by  
637 local sea-ice anomalies. Conversely, a less consistent picture is evident for the negative  
638 GBI events in spring.

639         Whatever the dominant mechanism(s) of the recent record (e.g. October, mid-  
640 2000s) GBI events and long-term positive summer GBI trend, we anticipate that our  
641 new daily GBI record will be useful for various further meteorological/climatological  
642 and glaciological studies of the recently observed rapid changes on the Greenland Ice  
643 Sheet, and will help to set recent extreme events (e.g. the extreme melts of 2012 and  
644 2015) in a longer-term climatic context, as well as helping to unravel new aspects of  
645 atmospheric forcing mechanisms of Greenland change. It will also be important to

646 examine the fidelity of Greenland blocking in climate-model projections (e.g.  
647 CMIP5/6), so that they can better represent past, present and future Greenland Blocking  
648 (and associated NAO) changes. Greenland blocking is intrinsically connected to GrIS  
649 mass balance (Hanna et al. 2013, 2014, Hofer et al. 2017, van den Broeke et al. 2017)  
650 and, by extension, global sea-level changes. Greenland blocks are importantly  
651 associated with meteorological/climatological effects and impacts downstream and  
652 further south (e.g. over Northwest Europe). Fully homogenised, updated daily GBI time  
653 series will be made available (on publication) from: <http://staff.lincoln.ac.uk/ehanna>

654

655

656

## 657 **Acknowledgements**

658

659 We thank the Met Office for provision of CET and EWP data. We acknowledge the  
660 NOAA ESRL PSD for the provision of NCEP/NCAR and 20CRV2c reanalysis data,  
661 and the CPC for NAO data. Support for the Twentieth Century Reanalysis Project  
662 dataset is provided by the U.S. Department of Energy, Office of Science Innovative and  
663 Novel Computational Impact on Theory and Experiment program, and Office of  
664 Biological and Environmental Research, and by the National Oceanic and Atmospheric  
665 Administration Climate Program Office. We thank three anonymous reviewers whose  
666 comments helped improve the manuscript.

667

668

669

670

671

672

673

674

675

676

677

678

679

680

681 **References**

682

683 Abramowitz, M., I.A. Stegun (1965) *Handbook of Mathematical Functions: with*  
684 *Formulas, Graphs, and Mathematical Tables*. Dover Books on Mathematics.

685 Alexander, L.V., P.D. Jones (2001) Updated precipitation series for the U.K. and  
686 discussion of recent extremes. *Atmos. Sci. Lett.*, doi:10.1006/asle.2001.0025.

687 Baggett, C., S. Lee (2017) An identification of the mechanisms that lead to Arctic  
688 warming during planetary-scale and synoptic-scale wave life cycles. *J. Atmos. Sci.*  
689 74, 1859-1877.

690 Ballinger, T.J., E. Hanna, R.J. Hall, J. Miller, M.H. Ribergaard, J.L. Høyer  
691 (2018a) Greenland coastal air temperatures linked to Baffin Bay and Greenland Sea  
692 ice conditions during autumn through regional blocking patterns. *Clim. Dyn.*, 50, 83-  
693 100.

694 Ballinger, T.J., E. Hanna, R.J. Hall, T.E. Cropper, J. Miller, M.H. Ribergaard, J.E.  
695 Overland, J.L. Høyer (2018b) Anomalous blocking over Greenland preceded the  
696 2013 extreme early melt of local sea ice. *Ann. Glaciol.*, in press.

697 Barnes, E.A., J. Screen (2015) The impact of Arctic warming on the midlatitude  
698 jetstream: Can it? Has it? Will it? *WIREs Clim. Change* 6, doi: 10.1002/wcc.337.

699 Barnston, A.G., R.E. Livezey (1987) Classification, seasonality and persistence of low-  
700 frequency atmospheric circulation patterns. *Mon. Wea. Rev.* 115, 1083-1126.

701 Barriopedro, D., R. García-Herrera, A.R. Lupo, E. Hernández (2008) A climatology of  
702 Northern Hemisphere blocking. *J. Clim.* 19, 1042-1063.

703 Benedict, J.J., S. Lee, S.B. Feldstein (2004) Synoptic view of the North Atlantic  
704 Oscillation. *J. Atmos. Sci.* 61, 121-144.

705 Bonne, J.-L., H.C. Steen-Larsen, C. Risi, M. Werner, H. Sodemann, J.-L. Lacour, X.  
706 Fettweis, G. Cesana, M. Delmotte, O. Cattani, P. Vellelonga, H.A. Kjaer, C.  
707 Clerbaux, A.E. Sveinbjörnsdóttir, V. Masson-Delmotte (2015) The summer 2012  
708 Greenland heat wave: In situ and remote sensing observations of water vapor  
709 isotopic composition during an atmospheric river event. *J. Geophys. Res. Atmos.* 120,  
710 2970-2989.

711 Budikova, D., T.W. Ford, T.J. Ballinger (2017) Connections between north-central  
712 United States summer hydroclimatology and Arctic sea ice variability. *Int. J. Climat.*  
713 367, 4434-4450.

714 Chen, X., and D. Luo (2017) Arctic sea ice decline and continental cold anomalies:  
715 Upstream and downstream effects of Greenland blocking. *Geophys. Res. Lett.* 44,  
716 3411–3419.

717 Compo, G.P. et al. (2011) The Twentieth Century Reanalysis project. *Q.J.R. Meteorol.*  
718 *Soc.* 137, 1-28.

719 Compo, G.P. et al. (2015) NOAA/CIRES Twentieth Century Global Reanalysis Version  
720 2c. Research Data Archive at the National Center for Atmospheric Research,  
721 Computational and Information Systems Laboratory.  
722 <http://rda.ucar.edu/datasets/ds131.2/> (accessed 8 January 2016).

723 Cropper, T.E., E. Hanna, M.A. Valente, T. Jonsson (2015) A daily Azores–Iceland  
724 North Atlantic Oscillation index back to 1850. *Geoscience Data Journal* 2, 12-24.

725 Davini, P., C. Cagnazzo, S. Gualdi, A. Navarra (2012a) Bidimensional diagnostics,  
726 variability, and trends of northern hemisphere blocking. *J. Clim.* 25, 6496-6509.

727 Davini, P., C. Cagnazzo, R. Neale, J. Tribbia (2012b) Coupling between Greenland  
728 blocking and the North Atlantic Oscillation pattern. *Geophys. Res. Lett.* 39, L14701.

729 DeWeaver, E. and S. Nigam (2000) Do stationary waves drive the zonal-mean jet  
730 anomalies of the northern winter? *J. Clim.* 13, 2160-2176.

731 Ding, Q., J.M. Wallace, D.S. Battisti, E.J. Steig, A.J.E. Gallant, H.-J. Kim, L. Geng  
732 (2014) Tropical forcing of the recent rapid Arctic warming in northeastern Canada  
733 and Greenland. *Nature* 509, 209-213.

734 Ding, Q., A. Schweiger, M. L’Heureux, D.S. Battisti, S. Po-Chedley, N.C. Johnson, E.  
735 Blanchard-Wrigglesworth, K. Harnos, Q. Zhang, R. Eastman, E.J. Steig (2017)  
736 Influence of high-latitude atmospheric circulation changes on summertime Arctic sea  
737 ice. *Nat. Clim. Change* 7, 289-295.

738 Duchon, C.E. (1979) Lanczos filtering in one and two dimensions. *J. Appl. Meteorol.*  
739 18, 1016-1022.

740 Fang, Z.-F. (2004) Statistical relationship between the northern hemisphere sea ice and  
741 atmospheric circulation during winter time. *In* *Observation, Theory and Modeling of*  
742 *Atmospheric Variability. World Scientific Series on Meteorology of East Asia*, Zhu,  
743 X. (Ed.) World Scientific Publishing Company: Singapore, 131–141.

744 Fenty, I., and P. Heimbach (2013) Coupled sea ice-ocean-state estimation in the  
745 Labrador Sea and Baffin Bay. *J. Phys. Oceanog.* 43, 884-904.

746 Franzke, C., S. Lee, S.B. Feldstein (2004) Is the North Atlantic Oscillation a breaking  
747 wave? *J. Atmos. Sci.* 61, 145-160.

748 Hall, R.J. (2016) *The North Atlantic Polar Front Jet Stream: Variability and*  
749 *Predictability, 1871-2014*. PhD thesis, University of Sheffield.

750 Hall, R.J., E. Hanna. (2018) North Atlantic circulation indices: links with summer and  
751 winter UK temperatures and precipitation and implications for seasonal forecasting.  
752 *Int. J. Climatol.*, doi: 10.1002/joc.5398.

753 Hall, R., R. Erdelyi, E. Hanna, J.M. Jones, A.A. Scaife (2015) Drivers of North Atlantic  
754 Polar Front jet stream variability. *Int. J. Climatol.* 35. 1697-1720.

755 Hanna, E., P. Huybrechts, K. Steffen, J. Cappelen, R. Huff, C. Shuman, T. Irvine-Fynn,  
756 S. Wise, M. Griffiths (2008) Increased runoff from melt from the Greenland Ice  
757 Sheet: a response to global warming. *J. Clim.* 21, 331-341.

758 Hanna, E., J. Cappelen, X. Fettweis, P. Huybrechts, A. Luckman, M.H. Ribergaard  
759 (2009) Hydrologic response of the Greenland ice sheet: the role of oceanographic  
760 warming. *Hydrol. Proc.* 23, 7-30.

761 Hanna, E., S.H. Mernild, J. Cappelen, K. Steffen (2012) Recent warming in Greenland  
762 in a long-term instrumental (1881-2012) climatic context: I. Evaluation of surface air  
763 temperature records. *Environ. Res. Lett.* 7, 045404.



764 Hanna, E., J.M. Jones, J. Cappelen, S.H. Mernild, L. Wood, K. Steffen, P. Huybrechts  
765 (2013) The influence of North Atlantic atmospheric and oceanic forcing effects on  
766 1900-2010 Greenland summer climate and ice melt/runoff. *Int. J. Climatol.* 33, 862-  
767 880.

768 Hanna, E., X. Fettweis, S.H. Mernild, J. Cappelen, M.H. Ribergaard, C.A. Shuman, K.  
769 Steffen, L. Wood, T.L. Mote (2014) Atmospheric and oceanic climate forcing of the  
770 exceptional Greenland ice sheet surface melt in summer 2012. *Int. J. Climatol.* 34,  
771 1022-1037.

772 Hanna, E., T.E. Cropper, P.D. Jones, A.A. Scaife, R. Allan (2015) Recent seasonal  
773 asymmetric changes in the NAO (a marked summer decline and increased winter  
774 variability) and associated changes in the AO and Greenland Blocking Index. *Int. J.*  
775 *Climatol.* 35, 2540-2554.

776 Hanna, E., T.E. Cropper, R.J. Hall, J. Cappelen (2016) Greenland Blocking Index 1851-  
777 2015: a regional climate change signal. *Int. J. Climatol.* 36, 4847-4861.

778 Hanna, E., R.J. Hall, J.E. Overland (2017) Can Arctic warming influence UK extreme  
779 weather? *Weather* 72, 346-352.

780 Hofer, S., A.J. Tedstone, X. Fettweis, J.L. Bamber (2017) Decreasing cloud cover  
781 drives the recent mass loss on the Greenland ice sheet. *Science Advances* 3,  
782 e1700584.

783 Kalnay, E. et al. (1996) The NCEP/NCAR 40-year reanalysis project. *Bull. Amer.*  
784 *Meteor. Soc.* 77, 437-470.

785 Liu, C., E. A. Barnes (2015), Extreme moisture transport into the Arctic linked to  
786 Rossby wave breaking. *J. Geophys. Res. Atmos.* 120, 3774–3788.

787 Luo, D., T. Gong, Y. Diao (2007a) Dynamics of eddy-driven low-frequency dipole  
788 modes. Part III: meridional displacement of westerly jet anomalies during two phases  
789 of NAO. *J. Atmos. Sci.* 64, 3232-3248.

790 Luo, D., A.R. Lupo, H. Wan (2007b) Dynamics of eddy-driven low-frequency dipole  
791 modes. Part I: A simple model of North Atlantic Oscillations. *J. Atmos. Sci.* 64, 3-28.

792 Markus T., J.C. Stroeve, J. Miller (2009) Recent changes in Arctic sea ice melt onset,  
793 freezeup, and melt season length. *J. Geophys. Res.* 114:C12024,  
794 doi:10.1029/2009JC005436.

795 Mattingly, K. S., J.T. McLeod, J.A. Knox, J.M. Shepherd, T.L. Mote (2015) A  
796 climatological assessment of Greenland blocking conditions associated with the track  
797 of Hurricane Sandy and historical North Atlantic hurricanes. *Int. J. Climatol.* 35,  
798 746–760.

799 McLeod, J., T. Mote (2015) Assessing the role of precursor cyclones on the formation  
800 of extreme Greenland blocking episodes and their impact on summer melting across  
801 the Greenland ice sheet. *J. Geophys. Res.* 120, 12357-12377.

802 McLeod, J.T., T.L. Mote (2016) Linking interannual variability in extreme Greenland  
803 blocking episodes to the recent increase in summer melting across the Greenland ice  
804 sheet. *Int. J. Climatol.* 36, 1484–1499.

805 Neff, W., G. P. Compo, F. M. Ralph, and M. D. Shupe (2014) Continental heat  
806 anomalies and the extreme melting of the Greenland ice surface in 2012 and 1889. *J.*  
807 *Geophys. Res.* 119, 6520–6536.

808 Orr, A., E. Hanna, J.C.R. Hunt, J. Cappelen, K. Steffen, A.G. Stephens (2005)  
809 Characteristics of stable flows over southern Greenland. *Pure and Applied*  
810 *Geophysics* 162, 1747-1778.

811 Overland, J.E., M. Wang (2015) Increased variability in early winter subarctic North  
812 American atmospheric circulation. *J. Clim.* 28, 7297–7305.

813 Overland, J. E., J.A. Francis, E. Hanna, M. Wang (2012) The recent shift in early  
814 summer Arctic atmospheric circulation. *Geophys. Res. Lett.* 39 (19).

815 Overland, J., J.A. Francis, R. Hall, E. Hanna, S.-J. Kim, T. Vihma (2015) The melting  
816 Arctic and midlatitude weather patterns: are they connected? *J. Clim.* 28, 7917-7932.

817 Overland, J.E., K. Dethloff, J.A. Francis, R.J. Hall, E. Hanna, S.-J. Kim, J.A. Screen,  
818 T.G. Shepherd, T. Vihma (2016) Nonlinear response of mid-latitude weather to the  
819 changing Arctic. *Nat. Clim. Change* 6, 992-999.

820 Park, H.-S., S. Lee, S.-W. Son, S.B. Feldstein, Y. Kosaka (2015) The impact of  
821 poleward moisture and sensible heat flux on Arctic winter sea ice variability. *J. Clim.*  
822 28, 5030-5040.

823 Parker, D.E., T.P. Legg, C.K. Folland (1992) A new daily Central England Temperature  
824 series, 1772-1991. *Int. J. Climatol.* 12, 317-342.

825 Parry, S., T. Marsh, M. Kendon (2013) 2012: from drought to floods in England and  
826 Wales. *Weather* 68, 268–274.

827 Priestley, M. D. K., J. G. Pinto, H. F. Dacre, L. C. Shaffrey (2017) Rossby wave  
828 breaking, the upper level jet, and serial clustering of extratropical cyclones in  
829 western Europe. *Geophys. Res. Lett.* 44, 514–521.

830 Rayner, N. A., D. E. Parker, E. B. Horton, C. K. Folland, L. V. Alexander, D. P.  
831 Rowell, E. C. Kent, A. Kaplan (2003) Global analyses of sea surface temperature,  
832 sea ice, and night marine air temperature since the late nineteenth century. *J.*  
833 *Geophys. Res.* 108, 4407.

834 Rex, D.F. (1950) Blocking action in the middle troposphere and its effect upon regional  
835 climate. *Tellus* 2, 196-211.

836 Rimbu, N., G. Lohmann, M. Werner, M. Ionita (2017) Links between central Greenland  
837 stable isotopes, blocking and extreme climate variability over Europe at decadal to  
838 multidecadal time scales. *Clim. Dyn.* 49, 649-663.

839 Scorer, R.S. (1988) Sunny Greenland. *Q.J. Roy. Meteorol. Soc.* 114, 3-29.

840 Serreze, M., J. Stroeve (2015) Arctic sea ice trends, variability and implications for  
841 seasonal forecasting. *Philosophical Transactions of the Royal Society A* 373:  
842 20140159.

843 Tedesco, M., T. Mote, X. Fettweis, E. Hanna, J. Jeyaratnam, J.F. Booth, R. Datta, K.  
844 Briggs (2016a) Arctic cut-off high drives the poleward shift of a new Greenland  
845 melting record. *Nat. Comm.* 7 (11723).

846 Tedesco, M., S. Doherty, X. Fettweis, P. Alexander, J. Jeyaratnam, J. Stroeve (2016b)  
847 The darkening of the Greenland ice sheet: trends, drivers, and projections (1981–  
848 2100). *The Cryosphere* 10, 477-496.

849 Titchner, H. A., N. A. Rayner (2014) The Met Office Hadley Centre sea ice and sea  
850 surface temperature data set, version 2: 1. Sea ice concentrations. *J. Geophys. Res.*  
851 *Atmos.* 119, 2864–2889.

852 Trenberth, K.E., J.T. Fasullo, G. Branstator, A.S. Phillips (2014) Seasonal aspects of the  
853 recent pause in surface warming. *Nat. Clim. Change* 4, 911-926.

854 van den Broeke, M. R., J. Box, X. Fettweis, E. Hanna, B. Noël, M. Tedesco, D. van As,  
855 W. J. van de Berg and L. van Kampenhout (2017) Greenland ice sheet surface mass  
856 loss: recent developments in observation and modelling. *Current Climate Change*  
857 *Reports*, [doi.org/10.1007/s40641-017-0084-8](https://doi.org/10.1007/s40641-017-0084-8).

- 858 Woollings, T., B. Hoskins, M. Blackburn, P. Berrisford (2008) A new Rossby wave-  
859 breaking interpretation of the North Atlantic Oscillation. *J. Clim.* 65, 609-626.
- 860 Woollings, T., A. Hannachi, B. Hoskins (2010) Variability of the North Atlantic eddy-  
861 driven jet stream. *Q.J. Roy. Meteorol. Soc.* 136, 856-868.
- 862 Yoo, C., S. Lee, S.B. Feldstein (2012) Mechanisms of Arctic surface air temperature  
863 change in response to the Madden-Julian Oscillation. *J. Clim.* 25, 5777-5790.

864 **Table 1.** Mean numbers of days per calendar month and season with **GBI values > 1** for specified decades and other periods. Highest  
 865 values for each month and season are emboldened. Recent climatological values are highlighted in grey.

Month/ season	1981- 2010	2006- 2015	2000- 2009	1990- 1999	1980- 1989	1970- 1979	1960- 1969	1950- 1959	1940- 1949	1930- 1939	1920- 1929	1910- 1919	1900- 1909	1851- 1899
Jan	2.9	3.7	3.4	1.2	4.2	4.2	<b>8.5</b>	5.4	5.9	3.6	2.7	3.9	1.3	3.2
Feb	4.6	6.2	5.7	1.6	4.9	2.9	7.6	5.7	<b>7.8</b>	5.1	1.5	2.2	6.5	3.7
Mar	5.2	7.8	5.8	5.2	4.4	4.5	3.8	7.2	5.5	7.5	4.9	7.1	<b>7.6</b>	5.5
Apr	5.1	4.4	3.3	<b>7.5</b>	3.7	6.0	3.1	5.0	2.4	2.3	4.8	2.0	3.5	4.0
May	5.5	6.6	5.9	5.7	4.8	4.8	3.9	<b>6.9</b>	3.8	4.1	5.5	1.7	6.3	3.3
Jun	7.1	<b>11.2</b>	8.0	7.0	5.5	2.9	1.4	7.1	5.4	5.2	6.9	6.2	8.0	4.9
Jul	6.3	<b>12.7</b>	10.1	6.5	2.3	6.0	6.1	5.1	5.1	7.4	3.0	11.2	4.1	6.0
Aug	5.2	<b>11.7</b>	7.8	2.4	5.1	4.7	7.6	5.7	3.4	5.8	4.1	6.8	3.5	5.3
Sep	6.3	5.2	5.3	7.1	5.4	3.7	4.5	4.9	2.8	<b>9.7</b>	4.3	6.0	5.1	5.8
Oct	7.2	8.9	<b>9.7</b>	6.4	5.1	5.6	4.6	2.9	6.2	4.6	5.6	4.9	4.3	8.4
Nov	4.6	2.9	3.0	5.6	5.0	1.4	5.3	5.1	5.9	2.2	4.2	5.7	5.8	<b>6.5</b>
Dec	6.1	7.0	7.1	3.6	5.8	4.8	<b>7.2</b>	5.3	4.6	5.5	4.4	3.5	2.5	4.4
ANN	66.1	<b>85.3</b>	75.1	59.8	56.2	51.5	63.6	66.3	58.8	63.0	51.9	61.2	58.5	61.1
JJA	18.6	<b>35.6</b>	25.9	15.9	12.9	13.6	15.1	17.9	13.9	18.4	14.0	24.2	15.6	16.2
DJF	13.0	17.2	13.9	7.4	14.2	12.0	<b>23.2</b>	16.1	19.1	13.4	8.6	10.1	10.8	11.3

866

867

868

869 **Table 2.** Linear trends in Greenland Blocking Index standard deviation of daily values,  
870 highest and lowest daily values, and numbers of days with GBI>0,1,2 for several  
871 months/seasons and different time periods. Units are normalised GBI values and (last  
872 three categories) numbers of days. Significant trends ( $p \leq 0.05$ ) are highlighted in bold.

Parameter	Month/season	1900-2015	1950-2015	1990-2015
GBI standard deviation of daily values	Jun	<b>-0.16</b>	0.00	-0.18
“	Jul	-0.14	<b>0.16</b>	-0.04
“	Dec	-0.01	0.07	-0.03
GBI highest daily value	Jun	-0.31	0.40	0.17
“	Jul	-0.17	0.44	<b>0.88</b>
“	Dec	0.17	0.55	0.12
GBI lowest daily value	Jun	0.35	0.23	<b>0.84</b>
“	Jul	<b>0.47</b>	0.11	<b>1.14</b>
“	Dec	0.31	0.15	0.33
No. of days with GBI>0	Jun	1.29	<b>7.35</b>	<b>10.81</b>
“	Jul	3.84	5.83	<b>14.25</b>
“	Dec	0.58	0.05	3.39
“	ANN	16.81	15.79	<b>65.62</b>
“	JJA	6.10	<b>15.74</b>	<b>38.84</b>
“	DJF	6.34	-3.32	<b>24.08</b>
No. of days with GBI>1	Jun	0.85	<b>6.37</b>	6.47
“	Jul	2.31	<b>5.98</b>	<b>8.76</b>
“	Dec	3.17	0.43	4.32
“	ANN	<b>14.42</b>	18.45	<b>43.11</b>
“	JJA	6.06	<b>15.23</b>	<b>28.50</b>
“	DJF	4.01	-4.46	13.37
No. of days with GBI>2	Jun	-0.37	1.27	1.90
“	Jul	-0.10	1.89	4.12
“	Dec	<b>1.59</b>	1.25	1.01
“	ANN	5.82	7.92	<b>19.62</b>
“	JJA	1.93	<b>5.58</b>	11.16
“	DJF	1.03	-0.09	4.76

873

874

875 **Table 3(a).** Rank-ordered summers (JJA) with the most number (nd) of GBI>1 days,  
 876 with corresponding numbers of days in those seasons reaching different GBI and NAO  
 877 thresholds, and means and standard deviations of daily GBI and NAO values.

878

<i>Year (JJA)</i>	<i>nd GBI&gt;1</i>	<i>nd GBI&gt;0</i>	<i>nd GBI&gt;2</i>	<i>nd NAO &lt;-1</i>	<i>nd NAO &lt;0</i>	<i>nd NAO &lt;-2</i>	<i>GBI mean</i>	<i>GBI stdev</i>	<i>NAO mean</i>	<i>NAO stdev</i>
2012	57	79	15	34	64	12	2.11	0.93	-0.59	1.39
2008	47	67	16	20	39	7	1.42	1.23	0.36	1.68
1887	44	77	11	30	53	16	1.64	0.89	-0.39	1.49
2011	44	83	16	15	52	1	1.58	0.84	-0.07	1.02
1895	39	64	13	29	58	18	1.17	1.14	-0.36	1.75
1877	38	67	13	33	50	20	1.20	1.17	-0.43	2.12
1911	38	66	7	41	55	26	1.21	1.06	-0.63	1.77
1912	38	69	5	27	57	12	0.97	1.04	-0.43	1.29
1931	38	66	15	30	45	14	1.41	1.07	-0.26	1.78
2007	38	80	8	26	45	16	1.55	0.76	-0.20	1.57
1891	37	65	14	38	63	23	1.23	1.13	-0.78	1.61
1893	37	84	13	40	65	28	1.71	0.83	-0.97	1.71
2009	37	74	11	31	50	16	1.43	0.96	-0.40	1.83

879

880

881

882

883

884

885

886

887

888



889 **Table 3(b).** Rank-ordered winters (DJF) with the most number (nd) of GBI>1 days,  
 890 with corresponding numbers of days in those seasons reaching different GBI and NAO  
 891 thresholds, and means and standard deviations of daily GBI and NAO values.

892

<i>Year (DJF)</i>	<i>nd GBI&gt;1</i>	<i>nd GBI&gt;0</i>	<i>nd GBI&gt;2</i>	<i>nd NAO &lt;-1</i>	<i>nd NAO &lt;0</i>	<i>nd NAO &lt;-2</i>	<i>GBI mean</i>	<i>GBI stdev</i>	<i>NAO mean</i>	<i>NAO stdev</i>
2010	59	79	25	63	76	43	2.12	0.99	-1.87	1.70
1969	42	73	13	63	75	30	1.57	0.88	-1.43	1.28
1960	37	56	12	38	57	24	0.99	1.11	-0.63	1.77
2011	37	57	19	46	61	31	1.20	1.49	-0.91	1.95
1879	36	61	16	41	60	28	1.28	1.19	-0.86	1.69
1881	36	69	2	58	71	33	1.06	0.91	-1.60	1.77
1936	36	76	0	57	73	22	1.26	0.64	-1.14	1.31
1855	34	66	3	49	72	31	0.88	0.88	-1.30	1.48
1941	34	59	5	42	63	20	0.91	1.04	-0.71	1.63
1940	33	69	11	42	72	21	1.20	0.99	-1.01	1.27
1947	32	50	13	36	56	14	0.72	1.24	-0.46	1.75
1895	31	64	6	45	61	26	1.02	0.92	-1.13	2.06
1901	31	41	17	35	56	18	0.50	1.33	-0.44	1.64

893

894

895

896

897

898

899

900

901

902

903

904

905 **Table 4.** De-trended correlation coefficients between numbers of days/month above or  
906 below stated GBI thresholds and (a) monthly mean GBI, (b) monthly mean NAO, and  
907 (c) numbers of days/month above and below NAO threshold of opposite sign and value.  
908 Finally (d) compares numbers of moderate and extreme NAO days with monthly mean  
909 GBI values. All the above are based on 1851-2015 data (see main text, Section 2, for  
910 dataset details). All values above 0.2 or below -0.2 are statistically significant ( $p < 0.01$ );  
911 red type denotes insignificant values.  
912

<b>(a)</b>	Month	<u>GBI&gt;2</u>	<u>GBI&gt;1</u>	<u>GBI&gt;0</u>	<u>GBI&lt;-1</u>	<u>GBI&lt;-2</u>
<b>GBI</b>	Jan	0.63	0.86	0.92	-0.72	-0.28
“	Feb	0.65	0.88	0.94	-0.81	-0.23
“	Mar	0.62	0.87	0.93	-0.74	-0.50
“	Apr	0.40	0.75	0.91	-0.87	-0.53
“	May	0.77	0.77	0.90	-0.78	-0.47
“	Jun	0.65	0.85	0.93	-0.76	-0.34
“	Jul	0.63	0.87	0.92	-0.77	-0.53
“	Aug	0.67	0.85	0.92	-0.73	-0.47
“	Sep	0.62	0.85	0.92	-0.74	-0.37
“	Oct	0.68	0.90	0.90	-0.71	-0.40
“	Nov	0.60	0.85	0.91	-0.74	-0.43
“	Dec	0.66	0.89	0.92	-0.73	-0.21
“	ANN	0.72	0.88	0.90	-0.77	-0.48
“	JJA	0.71	0.87	0.93	-0.78	-0.43
“	DJF	0.67	0.90	0.92	-0.79	-0.34
<b>(b)</b>	Month	<u>GBI&gt;2</u>	<u>GBI&gt;1</u>	<u>GBI&gt;0</u>	<u>GBI&lt;-1</u>	<u>GBI&lt;-2</u>
<b>NAO</b>	Jan	-0.53	-0.77	-0.74	0.44	<b>0.16</b>
“	Feb	-0.58	-0.78	-0.81	0.66	<b>0.14</b>
“	Mar	-0.52	-0.71	-0.75	0.59	0.36
“	Apr	-0.23	-0.48	-0.66	0.54	0.30
“	May	-0.52	-0.52	-0.65	0.53	0.34
“	Jun	-0.45	-0.59	-0.67	0.51	0.27
“	Jul	-0.33	-0.45	-0.29	0.20	<b>0.15</b>
“	Aug	-0.41	-0.52	-0.46	<b>0.12</b>	<b>0.05</b>
“	Sep	-0.43	-0.54	-0.57	0.34	<b>0.19</b>
“	Oct	-0.51	-0.63	-0.63	0.49	0.22
“	Nov	-0.40	-0.66	-0.73	0.53	0.23
“	Dec	-0.66	-0.74	-0.70	0.49	<b>0.12</b>
“	JJA	-0.33	-0.44	-0.38	<b>0.13</b>	<b>0.06</b>

“	DJF	-0.65	-0.81	-0.75	0.54	0.21
<b>(c)</b>	<u>Month</u>	<u>GBI&gt;2</u>	<u>GBI&gt;1</u>	<u>GBI&gt;0</u>	<u>GBI&lt;-1</u>	<u>GBI&lt;-2</u>
<b>Ndays NAO&lt;-2,- 1,0;&gt;1,2.</b>	Jan	0.52	0.77	0.75	0.52	0.26
“	Feb	0.64	0.80	0.82	0.70	0.20
“	Mar	0.56	0.73	0.77	0.63	0.42
“	Apr	0.16	0.48	0.66	0.55	0.30
“	May	0.43	0.43	0.61	0.59	0.39
“	Jun	0.49	0.59	0.69	0.54	0.32
“	Jul	0.29	0.43	0.34	0.23	0.22
“	Aug	0.42	0.49	0.47	0.11	0.00
“	Sep	0.38	0.54	0.58	0.32	0.25
“	Oct	0.52	0.62	0.63	0.52	0.26
“	Nov	0.39	0.67	0.74	0.58	0.28
“	Dec	0.76	0.74	0.70	0.55	0.14
“	ANN	0.51	0.57	0.64	0.45	0.23
“	JJA	0.40	0.44	0.44	0.20	0.09
“	DJF	0.71	0.80	0.77	0.61	0.27

913

<b>(d)</b>	<u>Month</u>	<u>NAO&lt;-2</u>	<u>NAO&lt;-1</u>	<u>NAO&lt;0</u>	<u>NAO&gt;1</u>	<u>NAO&gt;2</u>
<b>GBI</b>	Jan	0.70	0.76	0.79	-0.75	-0.59
“	Feb	0.72	0.80	0.84	-0.78	-0.66
“	Mar	0.64	0.75	0.79	-0.75	-0.65
“	Apr	0.42	0.54	0.61	-0.61	-0.52
“	May	0.54	0.54	0.62	-0.65	-0.59
“	Jun	0.50	0.63	0.66	-0.66	-0.52
“	Jul	0.24	0.34	0.39	-0.36	-0.31
“	Aug	0.45	0.44	0.45	-0.40	-0.25
“	Sep	0.48	0.56	0.57	-0.50	-0.38
“	Oct	0.62	0.63	0.65	-0.63	-0.50
“	Nov	0.57	0.70	0.73	-0.71	-0.54
“	Dec	0.68	0.72	0.74	-0.67	-0.61
“	ANN	0.49	0.50	0.49	-0.48	-0.39
“	JJA	0.34	0.37	0.39	-0.37	-0.23
“	DJF	0.72	0.78	0.79	-0.76	-0.66

914

915

916

917

918

919 **Table 5(a).** Anomalously high GBI events ( $\geq 3\sigma$  for  $\geq 3$  consecutive days), with concomitant NAO values, in reverse chronological order.  
 920 Lag between GBI peak and NAO trough, and mean and extreme CET/EWP values during these dates, are also given; \*extreme values are  
 921 within  $\pm 5$  days of the respective peak GBI dates. Several closely-spaced recent events that occurred during consecutive Octobers between  
 922 2002 and 2006 are highlighted in green. Mean CET anomalies (EWP values)  $< -1\sigma$  ( $> 2$  mm) are highlighted in blue; mean CET anomalies  
 923  $> +1\sigma$  are highlighted in yellow.  
 924

Dates	Mean GBI value for period	Highest GBI value in period	Mean C15 NAO value	Lowest C15 NAO value in period	C15 (CPC) NAO lag wrt GBI	Mean CET anomaly ( $\sigma$ )	Greatest CET anomaly ( $\sigma$ )	Mean daily EWP (mm)	Max daily EWP (mm)
2010 Dec 15-21	3.78	5.10	-3.48	-4.19	0&5 (2)	-2.26	-3.53	1.39	3.74
2010 Nov 25-27	3.45	3.61	-3.50	-3.57	1 (0&4)	-2.20	*-3.13	1.14	*3.40
2010 Aug 19-21	3.31	3.50	-1.36	-1.75	0 (0)	0.56	1.23	4.34	*21.33
2010 Jan 2-4	3.19	3.34	-3.86	-5.05	0 (0)	-1.49	-2.27	1.00	*4.06
2009 Jul 16-18	3.12	3.17	0.69	0.05	4 (-2)	-0.28	*-0.79	11.32	20.09
2006 Oct 16-20	3.63	4.29	-2.73	-3.73	-1 (3)	1.55	*2.03	4.99	*12.90
2006 May 9-11	3.07	3.12	-2.75	-3.08	3 (0)	1.49	1.73	0.42	*8.36
2005 Oct 18-21	3.38	3.54	-1.53	-2.01	-2 (2)	0.71	*1.85	7.14	*20.37
2003 Oct 17-20	3.54	3.84	-2.50	-3.17	0 (2)	-0.58	*-2.81	0.32	*5.20
2002 Oct 16-21	3.42	3.91	-4.02	-7.24	1 (3)	-1.28	-2.21	6.24	*21.52
1997 Nov 30- Dec 2	3.21	3.38	-2.04	-2.28	0 (-1)	-0.54	*-1.54	3.33	9.96
1995 Apr 25-27	3.20	3.40	-3.52	-4.07	0 (-1)	0.32	2.16	0.33	*8.59

1964 Aug 13-15	3.40	3.57	-3.46	-3.96	-1 (0)	-0.18	*-2.14	1.57	*10.45
1944 Jul 22-25	3.34	3.76	-3.80	-4.38	1	-0.38	*-1.17	0.60	*3.87
1929 Jan 26-28	4.06	4.49	-4.09	-4.42	0	-1.30	-1.63	N/A	N/A
1919 Jul 21-23	3.63	3.89	-0.74	-1.51	3	-1.05	*-2.00	N/A	N/A
1918 Jul 20-22	3.64	3.84	-1.51	-2.08	-5	-0.19	-1.26	N/A	N/A
1916 Sep 28- Oct 1	3.22	3.40	-3.10	-3.80	0	-0.00	*1.77	N/A	N/A
1902 Jul 22-24	3.44	3.56	-3.75	-4.38	0	-1.52	*-2.57	N/A	N/A
1900 Mar 24-26	3.39	3.73	-2.62	-3.25	0	-1.89	-2.05	N/A	N/A
1899 Dec 28-31	3.26	3.38	-2.55	-3.16	-1	-0.14	*-2.04	N/A	N/A
1897 Jun 5-7	3.19	3.28	-2.97	-3.19	-1	1.09	*1.96	N/A	N/A
1895 Oct 20-23	3.42	3.82	-5.16	-5.76	1	-1.75	*-3.59	N/A	N/A
1894 May 18- 20	3.65	3.93	-2.34	-2.65	0	-1.23	*-2.80	N/A	N/A
1888 Sep 29- Oct 3	3.57	4.27	-3.83	-5.14	0	-2.19	-4.00	N/A	N/A
1880 Oct 18-22	3.44	3.62	-4.47	-5.40	0	-2.27	-3.23	N/A	N/A
1880 Sep 30- Oct 4	3.69	3.88	-4.90	-6.64	1	-0.94	-2.80	N/A	N/A
1878 Dec 10-14	3.30	3.63	-2.89	-3.44	-1 & +6	-2.56	-3.27	N/A	N/A
1878 Nov 3-8	3.74	4.14	-2.48	-3.11	-8	-1.85	*-1.95	N/A	N/A
1876 Aug 22-24	3.32	3.55	-0.36	-0.81	0	1.13	*3.32	N/A	N/A
1875 Jul 22-24	3.48	3.79	-3.97	-4.67	-1	-0.44	*-1.41	N/A	N/A
1851 Nov 30- Dec 2	3.18	3.41	-1.99	-2.35	-4	-1.26	*-1.81	N/A	N/A

925

926

927

928

929

930

931

932

933

934

935

936

937

938 **Table 5(b).** Anomalously low GBI events (generally  $<-2.5\sigma$  for  $\geq 3$  consecutive days but  $<-2.0\sigma$  for  $\geq 3$  consecutive days for 1990-2015),

939 with concomitant NAO values, in reverse chronological order. Extreme value nomenclature and colour coding are as for Table 5(a).

Dates	Mean GBI value for period	Lowest GBI value in period	Mean C15 NAO value	Highest C15 NAO value in period	C15 (CPC) NAO lag wrt GBI	Mean CET anomaly ( $\sigma$ )	Greatest CET anomaly ( $\sigma$ )	Mean daily EWP (mm)	Max daily EWP (mm)
2013 Apr 19-22	-2.19	-2.42	1.87	3.36	3 (3)	-0.33	*1.86	0.38	*3.15
2011 Apr 19-21	-2.25	-2.43	1.25	1.80	4 (-5,0,5)	2.17	*3.22	0.01	*0.94

2011 Apr 11-17	-2.31	-2.54	1.16	3.12	-3 (1)	0.81	*3.27	0.25	*0.89
2011 Apr 14-16	-2.52	-2.54	0.81	1.75	-3 (1)	1.08	*2.59	0.04	*0.89
2011 Apr 4-7	-2.44	-2.85	0.79	1.81	0? (1-2)	1.97	3.27	1.05	*6.54
1999 Aug 31- Sep 2	-2.65	-2.74	2.09	2.20	3 (1)	1.14	*2.21	0.04	*3.85
1993 Nov 9-13	-2.24	-2.45	2.55	3.79	-2 (-1)	-0.25	*-1.34	9.42	21.04
1993 Mar 14-18	-2.20	-2.49	0.93	2.58	0 (1)	1.52	1.86	0.43	*6.76
1991 Aug 25-27	-2.51	-2.81	0.96	1.51	0 (1 & -2)	0.85	*1.85	0.18	*5.27
1991 Aug 18-21	-2.05	-2.09	1.15	1.42	? (0)	0.14	*1.34	0.27	*5.27
1990 Apr 11-15	-2.43	-2.71	4.37	5.15	1 (0)	0.13	1.35	2.28	3.83
1990 Apr 12-14	-2.63	-2.71	4.10	5.15	1 (0)	0.10	1.35	3.33	3.83
1955 Sep 4-6	-2.86	-3.04	2.68	3.56	-1 (0)	0.60	*2.00	2.67	4.79
1935 Jul 10-13	-2.96	-3.05	2.49	3.25	-1 & 4	1.66	2.34	0.39	*4.31
1934 Apr 30- May 3	-2.97	-3.32	3.69	4.10	-1	0.61	*-0.88	0.24	*10.55
1929 Jul 11-13	-2.74	-2.98	0.49	0.86	-1	0.30	*2.23	N/A	N/A
1920 Jul 27-29	-2.82	-2.93	2.84	3.62	1	2.02	*2.64	N/A	N/A
1906 Apr 4-6	-2.94	-3.13	3.19	3.67	0	0.76	*-1.34	N/A	N/A
1897 Apr 13-15	-2.81	-2.93	4.06	4.97	0	0.37	1.10	N/A	N/A
1896 Nov 19-22	-2.63	-2.83	2.38	3.87	-2	-0.20	*-0.93	N/A	N/A
1876 Jun 1-3	-2.69	-2.75	2.86	3.40	3	0.13	*0.91	N/A	N/A
1855 Jul 21-23	-2.92	-3.20	1.00	3.05	0	0.50	1.84	N/A	N/A
1853 Aug 9-11	-2.62	-2.81	-1.55	-0.12	-2	-0.46	-1.61	N/A	N/A

940

941

942

943

944

945

946

947

948

949

950

951

952



953 **Figure captions**

954

955 **Figure 1.** Cumulative sum of daily GBI 1851-2015 time series for: (a) annual; and  
956 seasonal months in (b) winter, (c) spring, (d) summer and (e) autumn.

957

958 **Figure 2.** Annual, summer (JJA) and winter (DJF) seasonal series of GBI days per year  
959 of given thresholds ( $>0$ ,  $>1$ ,  $>2$ ), 1851-2015. Linear trendlines are fitted through the  
960 annual data.

961

962 **Figure 3.** Running de-trended correlation coefficients between daily GBI and NAO  
963 values, showing variations in mean daily correlations over the seasonal cycle  
964 (correlation calculated for 1 January for all years, then repeated for each day of year)  
965 based on Cropper et al. (2015) Azores-Iceland station NAO series and (a) 1851-2015  
966 and (b) 1950-2015 data. Panel (b) also includes GBI correlations with the 1950-2015  
967 CPC NAO index (dotted blue line). In panel (c), correlations between GBI and station-  
968 based NAO are calculated for 1851 for all days, then repeated for all years. In all cases,  
969 a 7-point Gaussian filter has been applied to the raw correlation values for each  
970 day/year. Horizontal dashed lines show the  $p \leq 0.05$  significance level for correlation  
971 coefficients.

972

973 **Figure 4.** Composite (mean) plots of anomalies of (a,b) 500 hPa geopotential height,  
974 (c,d) wind speed, (e,f) 850 hPa temperature, (g,h) sea-ice concentration, and (i,j) sea-

975 surface temperature for the five seasons/years with the highest numbers of GBI>1 days  
976 during 1851-2015. Plots a,c,e,g,i are for winter and b,d,f,h,j are for summer.

977

978 **Figure 5.** North Atlantic atmospheric circulation parameters during composite life  
979 cycles of various GBI episodes: (a) four (2002, 2003, 2005 and 2006) October *high* GBI  
980 episodes; (b) five (2 x 1880, 1888, 1895 & 1916) September/October *high* GBI  
981 episodes; (c) three (1964, 2009 & 2010) July/August *high* GBI episodes; (d) three (1997  
982 & 2 x 2010) NDJ *high* GBI episodes; (e) seven (1897, 1906, 1934, 1990, 1993, 2011 &  
983 2013) MAM *low* GBI episodes. See Table 5 for definitions of high and low thresholds  
984 (in caption) and for further details of these events.

985

986 **Figure 6.** Running de-trended correlation coefficients of daily (a,b) CET and (c,d) EWP  
987 with daily GBI and NAO values for 1851-2015 (CET) and 1931-2015 (EWP), including  
988 (a,c) variations in mean daily correlations over the seasonal cycle (correlation calculated  
989 for 1 January for all years, then repeated for each day of year) and (b,d) correlation  
990 calculated for 1851 (CET) and 1931 (EWP) for all days, then repeated for all years. A 7-  
991 point Gaussian filter has been applied to the raw correlation values for each day/year.  
992 Horizontal dashed lines show the  $p \leq 0.05$  significance level for correlation coefficients.

993

994

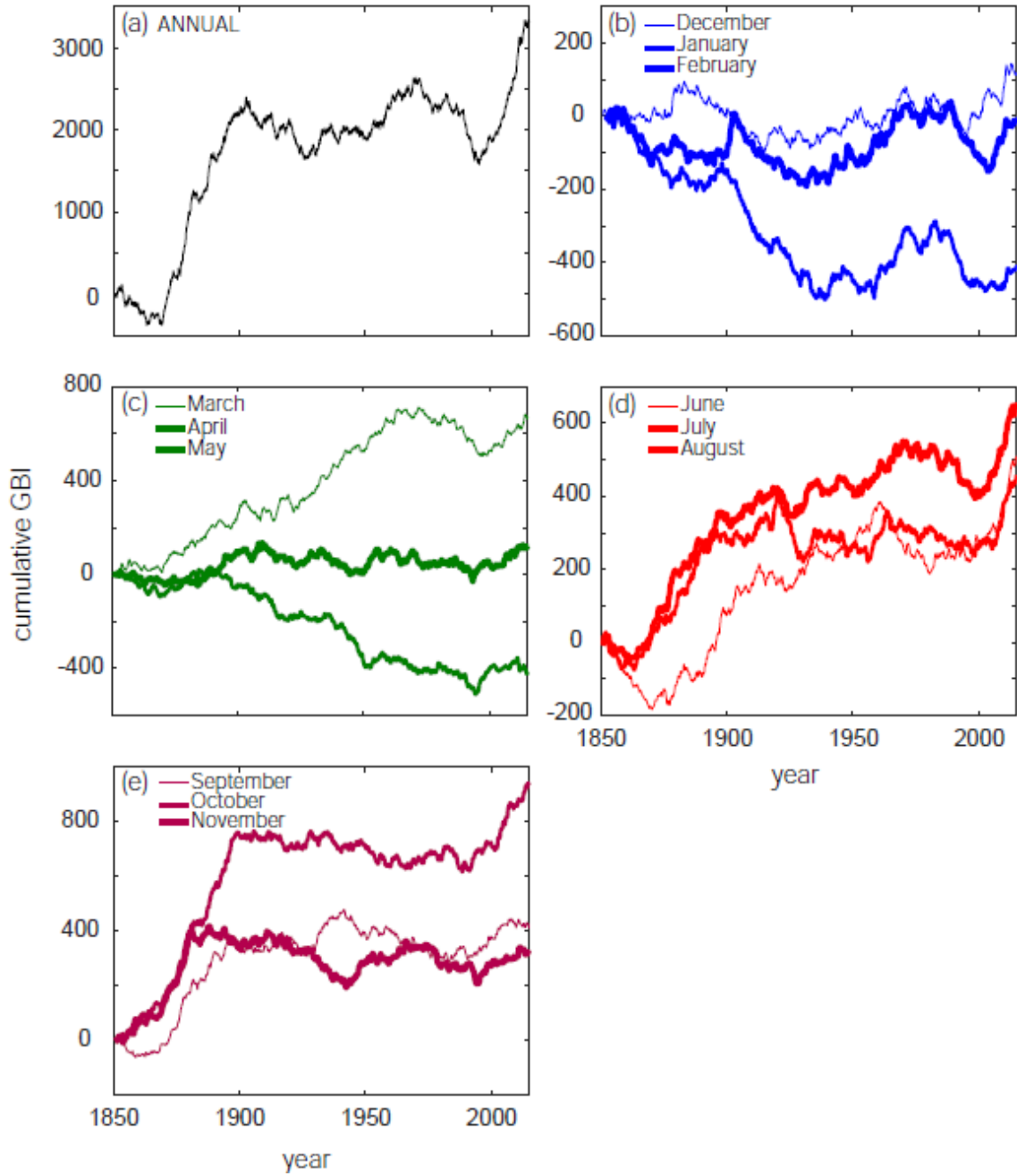
995

996

997

998

999 **Figure 1.** Cumulative sum of daily GBI 1851-2015 time series for: (a) annual; and  
 1000 seasonal months in (b) winter, (c) spring, (d) summer and (e) autumn.



1001

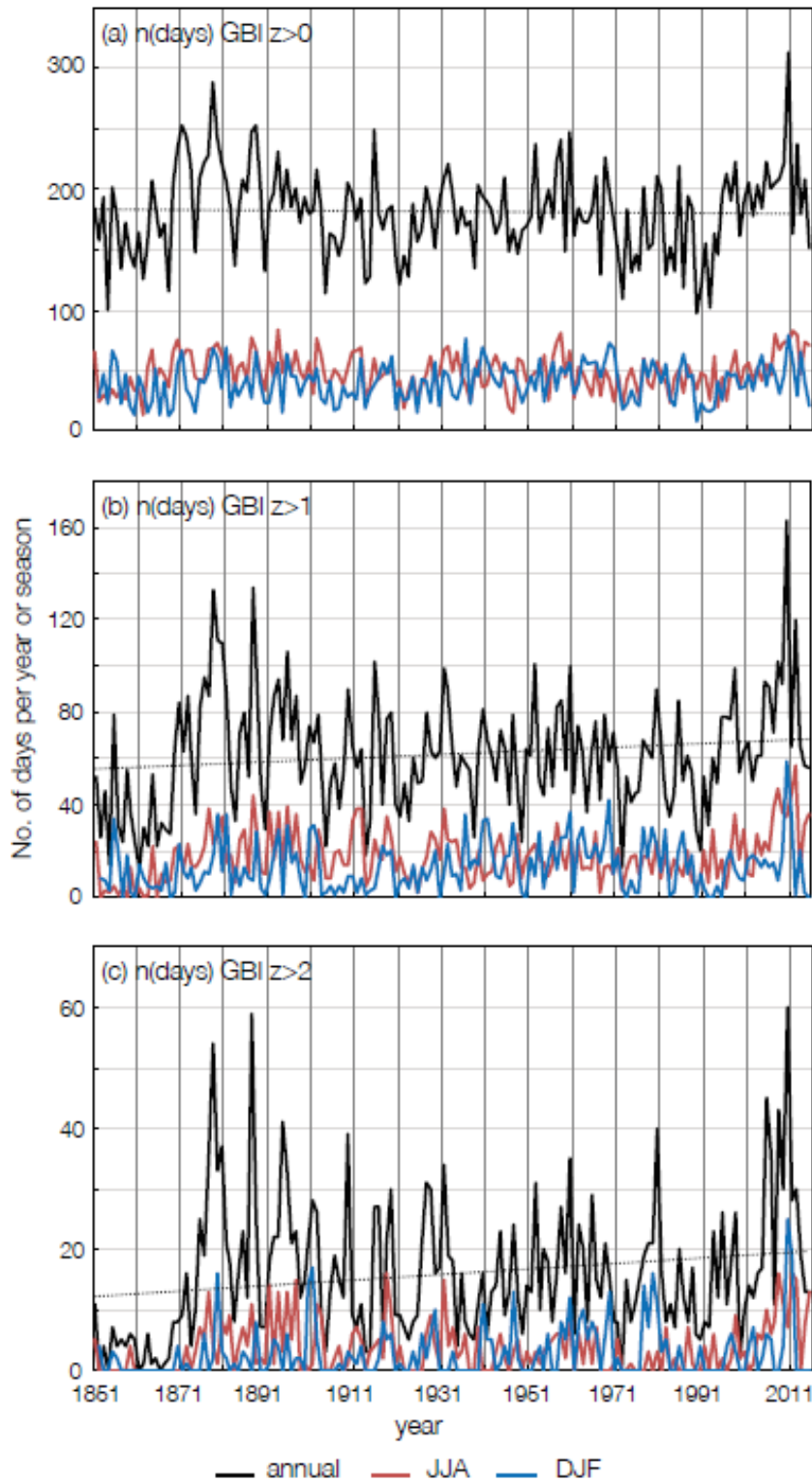
1002

1003

1004

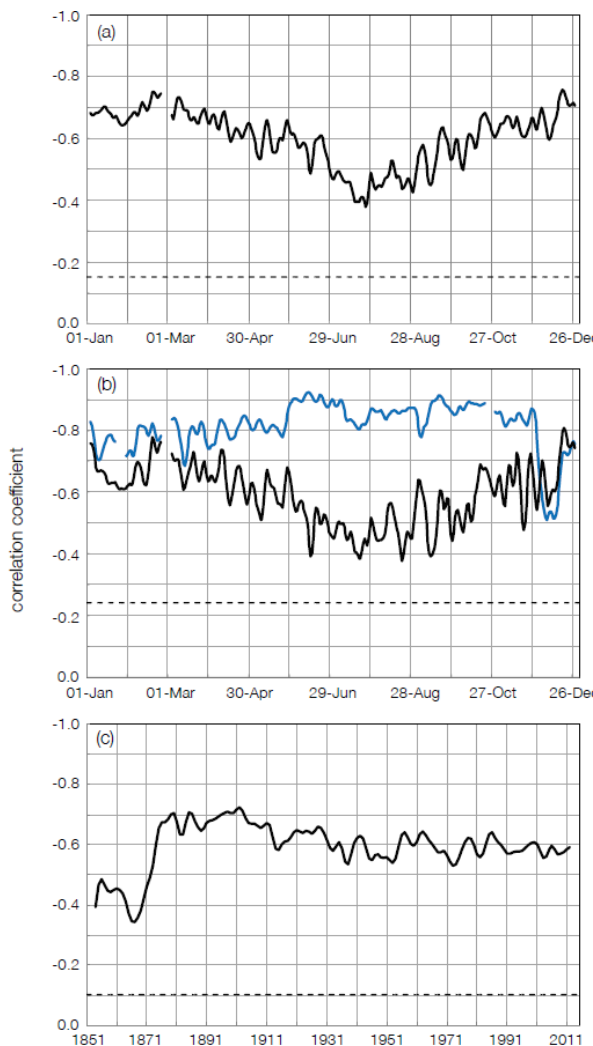
1005

1006 **Figure 2.** Annual, summer (JJA) and winter (DJF) seasonal series of GBI days per year  
 1007 of given thresholds ( $>0$ ,  $>1$ ,  $>2$ ), 1851-2015. Linear trendlines are fitted through the  
 1008 annual data.



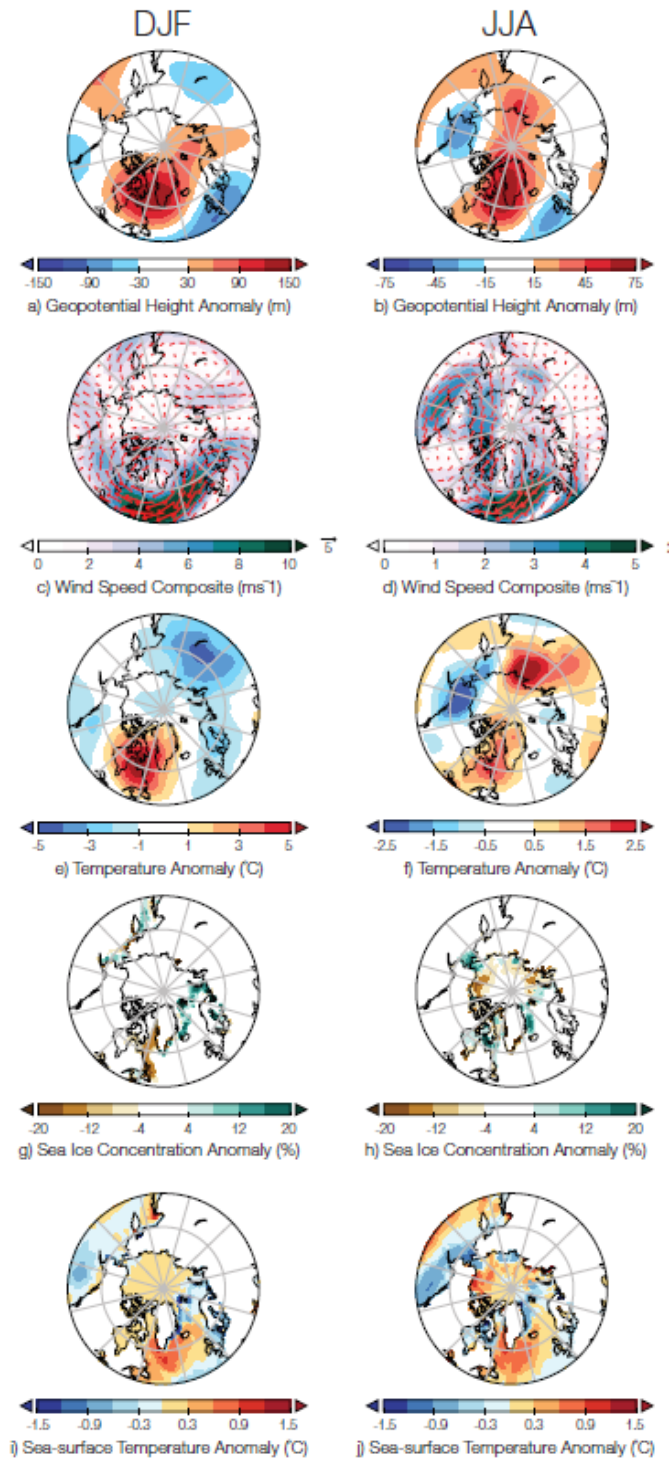
1009

1010 **Figure 3.** Running de-trended correlation coefficients between daily GBI and NAO  
 1011 values, showing variations in mean daily correlations over the seasonal cycle  
 1012 (correlation calculated for 1 January for all years, then repeated for each day of year)  
 1013 based on Cropper et al. (2015) Azores-Iceland station NAO series and (a) 1851-2015  
 1014 and (b) 1950-2015 data. Panel (b) also includes GBI correlations with the 1950-2015  
 1015 CPC NAO index (dotted blue line). In panel (c), correlations between GBI and station-  
 1016 based NAO are calculated for 1851 for all days, then repeated for all years. In all cases,  
 1017 a 7-point Gaussian filter has been applied to the raw correlation values for each  
 1018 day/year. Horizontal dashed lines show the  $p \leq 0.05$  significance level for correlation  
 1019 coefficients.



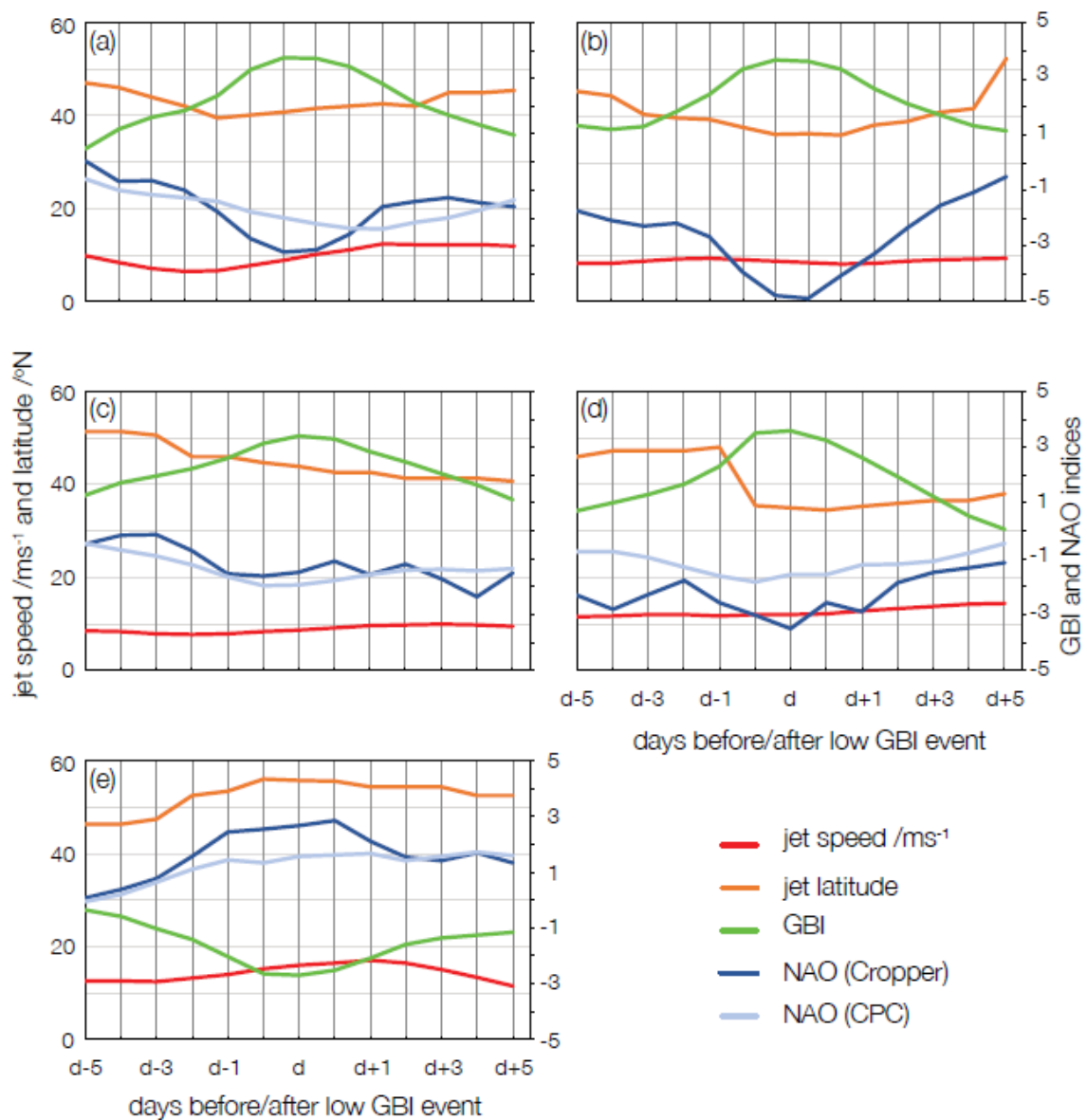
1020

1021 **Figure 4.** Composite (mean) plots of anomalies of (a,b) 500 hPa geopotential height,  
 1022 (c,d) wind speed, (e,f) 850 hPa temperature, (g,h) sea-ice concentration, and (i,j) sea-  
 1023 surface temperature for the five seasons/years with the highest numbers of GBI>1 days  
 1024 during 1851-2015. Plots a,c,e,g,i are for winter and b,d,f,h,j are for summer.



1025

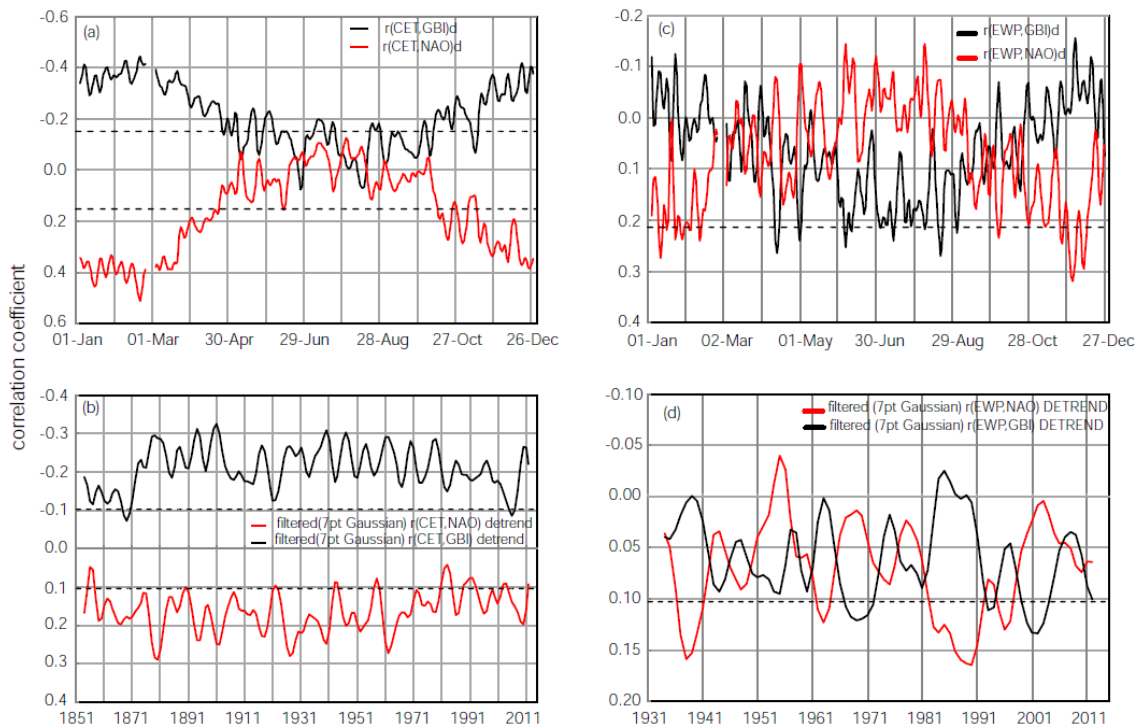
1026 **Figure 5.** North Atlantic atmospheric circulation parameters during composite life  
 1027 cycles of various GBI episodes: (a) four (2002, 2003, 2005 and 2006) October *high* GBI  
 1028 episodes; (b) five (2 x 1880, 1888, 1895 & 1916) September/October *high* GBI  
 1029 episodes; (c) three (1964, 2009 & 2010) July/August *high* GBI episodes; (d) three (1997  
 1030 & 2 x 2010) NDJ *high* GBI episodes; (e) seven (1897, 1906, 1934, 1990, 1993, 2011 &  
 1031 2013) MAM *low* GBI episodes. See Table 5 for definitions of high and low thresholds  
 1032 (in caption) and for further details of these events.



1033

1034

1035 **Figure 6.** Running de-trended correlation coefficients of daily (a,b) CET and (c,d) EWP  
 1036 with daily GBI and NAO values for 1851-2015 (CET) and 1931-2015 (EWP), including  
 1037 (a,c) variations in mean daily correlations over the seasonal cycle (correlation calculated  
 1038 for 1 January for all years, then repeated for each day of year) and (b,d) correlation  
 1039 calculated for 1851 (CET) and 1931 (EWP) for all days, then repeated for all years. A 7-  
 1040 point Gaussian filter has been applied to the raw correlation values for each day/year.  
 1041 Horizontal dashed lines show the  $p \leq 0.05$  significance level for correlation coefficients.



1042